NASA TECHNICAL NOTE

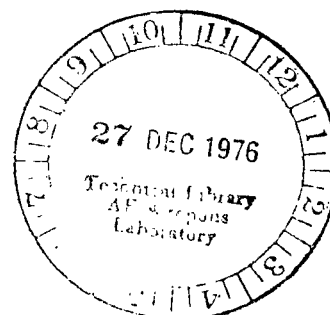NASA TN D-8350
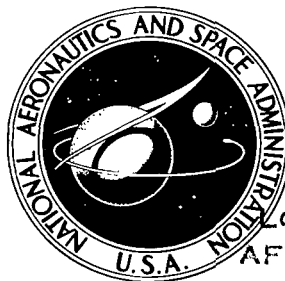
LOW-SPEED WIND-TUNNEL INVESTIGATION OF A LARGE-SCALE ADVANCED ARROW-WING SUPERSONIC TRANSPORT CONFIGURATION WITH ENGINES MOUNTED ABOVE WING FOR UPPER-SURFACE BLOWING

James P. Shivers, H. Clyde McLemore, and Paul L. Coe, Jr.

Langley Research Center
Hampton, Va. 23665

NATIONAL AERONAUTICS AND SPACE ADMINISTRATION • WASHINGTON, D. C. • DECEMBER 1976

1. Report No. NASA TN D-8350	2. Government Accession No.	3. Recipient's Catalog No.
4. Title and Subtitle LOW-SPEED WIND-TUNNEL INVESTIGATION OF A LARGE-SCALE ADVANCED ARROW-WING SUPERSONIC TRANSPORT CONFIGURATION WITH ENGINES MOUNTED ABOVE WING FOR UPPER-SURFACE BLOWING		5. Report Date December 1976
		6. Performing Organization Code
7. Author(s) James P. Shivers, H. Clyde McLemore, and Paul L. Coe, Jr.		8. Performing Organization Report No. L-10994
9. Performing Organization Name and Address NASA Langley Research Center Hampton, VA 23665		10. Work Unit No. 743-04-12-02
		11. Contract or Grant No.
12. Sponsoring Agency Name and Address National Aeronautics and Space Administration Washington, DC 20546		13. Type of Report and Period Covered Technical Note
		14. Sponsoring Agency Code

15. Supplementary Notes

16. Abstract

Tests have been conducted in the Langley full-scale tunnel to determine the low-speed aerodynamic characteristics of a large-scale advanced arrow-wing supersonic transport configuration with engines mounted above the wing for upper-surface blowing. Tests were made over an angle-of-attack range of -10° to 32°, sideslip angles of $\pm 5^\circ$, and a Reynolds number range of 3.53×10^6 to 7.33×10^6 (referenced to mean aerodynamic chord length of 3.368 m (11.050 ft) of the wing). Configuration variables included trailing-edge flap deflection, engine jet-nozzle angle, engine thrust coefficient, engine-out operation, and asymmetrical trailing-edge boundary-layer control for providing roll trim. Downwash measurements at the tail were obtained for different thrust coefficients, tail heights, and at two fuselage stations.

17. Key Words (Suggested by Author(s)) Aerodynamics Low speed stability and control Advanced supersonic transport	18. Distribution Statement Unclassified — Unlimited Subject Category 02

19. Security Classif. (of this report) Unclassified	20. Security Classif. (of this page) Unclassified	21. No. of Pages 59	22. Price* $4.25

LOW-SPEED WIND-TUNNEL INVESTIGATION OF A LARGE-SCALE ADVANCED ARROW-WING SUPERSONIC TRANSPORT CONFIGURATION WITH ENGINES MOUNTED ABOVE WING FOR UPPER-SURFACE BLOWING

James P. Shivers, H. Clyde McLemore, and Paul L. Coe, Jr.
Langley Research Center

SUMMARY

Tests have been conducted in the Langley full-scale tunnel to determine the low-speed aerodynamic characteristics of a large-scale advanced arrow-wing supersonic transport configuration with engines mounted above the wing for upper-surface blowing.

The results of the investigation indicated that the use of upper-surface blowing was effective for providing increased lift for improved take-off and landing performance. Although large diving moments accompanied the high propulsive lift, analysis indicated that an all-movable canard in combination with a relatively small conventional tail may be an effective arrangement for achieving low-speed longitudinal stability and trim. The model with tail on exhibited static directional stability up to an angle of attack of about 20° and had high positive effective dihedral. Large rolling and yawing moments were introduced with one engine inoperative; however, the use of the asymmetric boundary-layer control (BLC) on the trailing-edge flaps achieved roll trim for moderate angles of attack but excessively high values of flow coefficient were required. Spoiler deflection provided relatively large lateral control moments. The available approach lift coefficient could be increased by use of large angle flap deflection in conjunction with exhaust nozzle deflectors without requiring excessively high values of thrust-weight ratio.

INTRODUCTION

The present investigation was conducted to determine the low-speed performance and stability and control characteristics of an advanced arrow-wing supersonic transport configuration with engines mounted above the wing for upper-surface blowing (USB). The investigation was made as part of a general research program to provide a technology base for the formulation and development of an advanced supersonic transport configuration. Other investigations conducted as part of this program are reported in references 1 and 2.

Although the highly swept arrow-wing supersonic transport configuration is expected to be aerodynamically efficient at high speeds (refs. 3 and 4), past configurations of this

type have embodied several design features which result in poor take-off and landing per-formance. For example, the trailing-edge flaps were relatively ineffective because the conventional lower-surface engine arrangement occupied most of the inboard wing span and the flaps were therefore limited to small spanwise segments between the engines. The small flap segments and a relatively long fuselage, which restricted the ground rotation angle to 10° or less, resulted in maximum values of take-off and landing lift coefficients of only about 0.5. Because of the low values of lift coefficient, a wing area somewhat greater than that required for efficient cruise performance must be used in order to pro-vide acceptable take-off and landing speeds and runway lengths. One means of providing additional lift with a wing sized for efficient cruise is the use of the USB concept. In the USB concept, the engines, or possibly the inboard engines only for a four-engine arrange-ment, are located above the wing so that the exhaust flow can be deflected over the trailing-edge flaps. In such an arrangement, the trailing-edge flap span can be made continuous in order to achieve the maximum lift effectiveness.

The present investigation consisted of low-speed wind-tunnel tests conducted in the Langley full-scale tunnel for a range of Reynolds number, based on the mean aerodynamic chord of 3.368 m (11.050 ft), from 3.53×10^6 to 7.33×10^6 which corresponds to test velocities of about 15.48 m/s (50.8 ft/sec) to 31.94 m/s (104.8 ft/sec), respectively. The tests were conducted for a range of angles of attack from about -10° to 32° and sideslip angles of $\pm5^O$. The configuration variables included trailing-edge flap deflection, engine jet nozzle angle, and engine thrust coefficient. Also included in the investigation were tests to measure the forces and moments produced in the one-engine-inoperative condition. Tests were also conducted to examine the use of asymmetrical trailing-edge boundary-layer control (BLC) for providing roll trim in the one-engine-inoperative condition.

SYMBOLS

The longitudinal data are referred to the wind system of axes and the lateral-directional data are referred to the body system of axes illustrated in figure 1. The moment reference center for the tests was located at 53.8 percent of the wing mean aero-dynamic chord. The dimensional quantities herein were measured in U.S. Customary Units and are given both in the International System of Units (SI) and in U.S. Customary Units.

b   wing span, 4.191 m (13.750 ft)

C_D drag coefficient, $\dfrac{\text{Drag}}{qS}$

C_L lift coefficient, $\dfrac{\text{Lift}}{qS}$

$C_{L,t}$ lift coefficient at the tail

$C_{L,\Gamma}$ circulation lift coefficient

C_l rolling-moment coefficient, $\dfrac{\text{Rolling moment}}{qSb}$

C_m pitching-moment coefficient, $\dfrac{\text{Pitching moment}}{qS\bar{c}}$

C_n yawing-moment coefficient, $\dfrac{\text{Yawing moment}}{qSb}$

C_Y side-force coefficient, $\dfrac{\text{Side force}}{qS}$

C_μ blowing coefficient, $\dfrac{\text{Thrust produced by boundary-layer control}}{qS}$

c chord, m   (ft)

$\bar{c}$ mean aerodynamic chord, 3.368 m (11.050 ft)

F_A axial force, N   (lbf)

F_N normal force, N   (lbf)

i_c canard incidence, deg

i_t horizontal-tail incidence, positive when trailing edge is down, deg

L/D lift-drag ratio

l tail length, m   (ft)

q free-stream dynamic pressure, Pa   (lbf/ft^2)

S wing area, 10.232 m^2 (110.14 ft^2)

S_t tail or canard area, m^2 (ft^2)

T net engine thrust (thrust above value for $T_c' = 0$), N   (lbf)

T_c' thrust coefficient, T/qS

$T_c' = 0$ thrust coefficient corresponding to condition where engine exhaust total pressure equals free-stream total pressure

X   longitudinal body axis

y   distance along semispan, m (ft)

z   distance above center of gravity, m (ft)

α angle of attack, deg

β angle of sideslip, deg

δ_f trailing-edge flap deflection, positive when trailing edge is down, deg

δ_j static turning angle, deg, $\tan^{-1} \dfrac{F_N}{F_A}$

ϵ downwash angle, deg

η static turning efficiency, $\dfrac{\sqrt{F_N^2 + F_A^2}}{T}$

Derivatives:

$$C_{l_\beta} = \frac{\partial C_l}{\partial \beta} \qquad C_{n_\beta} = \frac{\partial C_n}{\partial \beta} \qquad C_{Y_\beta} = \frac{\partial C_Y}{\partial \beta}$$

MODEL

The dimensional characteristics of the model are listed in table I and shown in figure 2. A sketch of survey rake positions used in downwash measurements is shown in figure 3. Photographs of the model mounted for tests in the Langley full-scale tunnel are presented in figures 4 and 5. The model was constructed of wood and fiber glass over an aluminum frame and was essentially rigid for these low-speed tests.

The wing consisted of an arrow planform with an inboard leading-edge sweep angle of 74° to $\dfrac{y}{b/2} = 0.470$, then a midspan sweep angle of 70.5° to $\dfrac{y}{b/2} = 0.725$, and an outboard (27.5 percent of the semispan) sweep of 60°. It was mounted to the fuselage of the variable-sweep model discussed in reference 1. The wing (designed with twist and camber for a flight Mach number of 2.7) was constructed to simulate the shape of an elastic

wing in 1g flight at low speeds. The thickness ratio of the wing was 3.08 percent, and the outboard 27.5-percent semispan leading edge was drooped 45°. The outboard trailing edge was deflected downward 5°. The wing had plain trailing-edge flaps that extended from the fuselage to the outboard vertical fins. (See figs. 2(a) and 2(b).) A blowing slot, located forward of the leading edge of the left flap, was oriented to blow a sheet of high-pressure air over the upper surface of the two inboard flaps to control flow separation. (See fig. 2(c).) The trailing-edge flaps could be deflected from 0° to 30°.

The model was powered by two-engine simulators mounted forward on the wing upper surface. The engine simulators consisted of tip-driven fans which were powered with externally supplied compressed air. The conical nozzle exits could be configured with 20° or 30° eyelid deflectors for turning the exhaust flow downward onto the wing upper surface.

Although most of the tests were conducted with the model in a tail-off configuration, the T-tail of reference 1 was installed for a limited number of tests.

TESTS AND CORRECTIONS

Force tests were conducted in the Langley full-scale tunnel for a range of Reynolds numbers (based on the wing mean aerodynamic chord of 3.368 m (11.050 ft)) of 3.53×10^6 to 7.33×10^6. Tests were conducted at angles of attack from about -10° to 32°, and a few tests were conducted at sideslip angles of ±5°. Tests were conducted with flap angles of 0°, 10°, 20°, and 30°, with and without engines operating. The powered tests were made with and without deflectors attached to the engine exhaust nozzles. The value of thrust coefficient varied from 0 to 0.40; for a few tests, the left engine was inoperative while flap blowing $\left(\text{values of } C_{\mu} \text{ up to 0.10}\right)$ was applied to the left flap to determine whether flap blowing could be used for controlling an engine-out situation.

Although the arrow-wing model was planned for tail-off tests only, the T-tail of reference 1 was installed for a limited number of tests in order to determine preliminary longitudinal stability and control characteristics of the model. The desired tail position for the arrow-wing configuration would probably be somewhat further aft than that of the T-tail as tested.

Downwash flow surveys were made at two vertical planes in the vicinity of the T-tail. One plane was on the center line of the horizontal-tail pivot point ($l/\bar{c} = 0.982$); the other survey was made further aft at $l/\bar{c} = 1.254$. The survey covered a grid relative to a fixed body axis as indicated in figure 3 for four angles of attack. A calibrated pitch-yaw pitot-static tube was used to measure the flow angles.

The test data have been corrected for air-flow angularity, buoyancy, and strut tares. Wall corrections were found by theory of reference 5 to be negligible and were not applied.

RESULTS AND DISCUSSION

Longitudinal Characteristics

Static turning.- Since the effectiveness of a jet-flap system is dependent to a large extent upon the capability of the system to turn and spread the jet exhaust efficiently, static-turning tests were made of all the configurations included in the present investigation. The results are presented in figure 6 in terms of the ratio of normal force to thrust F_N/T plotted against the negative ratio of axial force to thrust F_A/T at zero angle of attack. The results of figure 6 show, as expected, that very little turning occurred without the use of exhaust deflectors. The best turning performance was achieved with the 20° deflectors as indicated by static turning efficiencies of 85 to 87 percent. The 30° deflectors gave poor static-turning characteristics, apparently because of excessive spreading which caused much of the jet exhaust to spread laterally off the flap.

Tail-off configuration.- Presented in figure 7 are the results of tests to determine the effect of variations in Reynolds number from 3.53×10^6 to 7.33×10^6 on the longitudinal characteristics of the wing-body combination. The data show that Reynolds number had only a small effect on the lift, drag, and pitching-moment characteristics of the model, particularly above a Reynolds number of 5.00×10^6. Most of the tests were made at a Reynolds number of about 5.00×10^6. The only exception is at $T_c' = 0.4$ where the Reynolds number was about 3.53×10^6.

Presented in figure 8 are the longitudinal characteristics of the wing-body combination for a range of thrust coefficients with the exhaust deflectors off. The data of figure 8(a) show that with the trailing-edge flaps undeflected, the effect of thrust was to increase the lift-curve slope so that at an angle near the ground-scrape angle (assumed to be 10° for this configuration), the lift coefficient was increased from about 0.4 to about 0.5 for $T_c' = 0.10$ and to C_L of about 0.55 for $T_c' = 0.20$. It is of interest to note that the increase in lift coefficient due to thrust is greater than that which could be accounted for by consideration of the direct component of the thrust vector $\left(T_c' \sin \alpha\right)$. Thus, the engine exhaust above the wing provided some additional circulation lift.

The pitching-moment data of figure 8(a) show the configuration to be neutrally stable at negative angles of attack and unstable at higher positive angles of attack, the level of instability increasing rapidly at angles of attack above about 15°. The abrupt increase in instability at the high angles of attack is similar to that shown for the highly swept configuration of previous studies (for example, see ref. 6) and is associated with the vortex lift generated on the forward part of the wing. This type of instability was eliminated in reference 6 by either deflecting the wing leading edge or by increasing the wing leading-edge radius. The data of figures 8(b) and 8(c) show similar effects of power for trailing-edge flap deflections of 10° and 20°.

The effects of installing exhaust deflectors on the model with trailing-edge flap deflections of 10° and 20° are shown in figures 9 and 10, respectively. A comparison of the data of figures 9 and 10 with those of figure 8 shows that, in general, the deflectors, as expected, increased the lift and generated large diving moments. The data of figures 9 and 10 show that the 20° and 30° exhaust deflectors gave about the same lift performance for a given geometric flap angle, and the 20° deflector provided slightly better thrust performance than that for the 30° deflector. This result is generally in agreement with the static-turning results of figure 6; although, based on the static-turning data, the 30° deflector would be expected to produce much lower lift than that actually generated in the wind-on test. From these data, it was concluded that the 20° deflectors were probably more suitable from overall considerations, and the remainder of the program was conducted with the 20° deflectors.

The data of figure 11 show that larger increments of lift were produced with 30° flap deflection than those for the 10° and 20° flap conditions. For example, at an angle of attack of 10°, a lift coefficient of about 0.9 was achieved with a thrust coefficient of 0.2 (fig. 11); whereas for the same thrust coefficient with 20° flap (fig. 10), a lift coefficient of about 0.8 was achieved. As expected, the increased lift provided by the higher flap angle setting produced larger diving moments and resulted in an increase in drag.

In order to better illustrate the effect of thrust in producing lift with the jet exhaust deflected downward over the trailing-edge flaps, the lift components which make up the total lift are presented in figure 12 for several trailing-edge flap deflections. The data of figure 12 show the values of circulation lift $\left(C_{L,\Gamma}\right)$ as a function of $T_c{}'$ for all flap deflections, and, as expected, the 30° flap showed higher values of $C_{L,\Gamma}$ than those produced by lower flap settings.

Downwash characteristics.- Presented in figures 13 and 14 are the results of flow surveys to measure the downwash characteristics at several different vertical positions where the horizontal tail could normally be located. The data show, in general, that the downwash angle was relatively small at the high tail positions. At the low tail position, the downwash angle was large, and the variation of downwash angle with lateral displacement was very pronounced. The data of figures 13 and 14 are summarized in figure 15 in terms of the downwash factor $1 - \dfrac{d\epsilon}{d\alpha}$ plotted against tail height. The data of figure 15 show that the low tail positions gave values of $1 - \dfrac{d\epsilon}{d\alpha}$ from about 0.1 to 0.2 and indicate that a low horizontal-tail position would be relatively ineffective from the standpoint of providing static longitudinal stability.

Tail-on configuration.- In order to provide some preliminary information on longitudinal control effectiveness, tests were made by using an existing vertical- and horizontal-tail assembly from the investigation reported in reference 1. The resulting control effectiveness data are presented in figure 16. It should be noted that the data are not

intended to be representative of the tail effectiveness for a properly configured arrow-wing arrangement, but the data should serve as a guide in an analysis of the tail size and location required for the configuration. The data of figure 16 show that the horizontal tail, which had an area of 5.8 percent of the wing area, provided a slight amount of longitudinal stability for the configuration in the low angle-of-attack range. Furthermore, the data of figure 16(a) show that a -10° control incidence angle provided trim for the 30° flap condition with $T_c' = 0$; but for values of T_c' of 0.1 and 0.2, the diving moments could not be trimmed.

Pitch trim consideration.- One of the problems associated with the use of the USB concept is that the lift loads induced on the flaps produce large diving moments. (See fig. 11.) The magnitude of the problem of trimming the diving moments is illustrated in figure 16 by the fact that a modest-sized conventional aft tail was inadequate for providing stability and trim for the powered-lift condition. Since the use of USB for high lift is dependent upon a satisfactory solution to the pitch trim problem, a brief analytical study was made of the relative merits of several methods of providing pitch trim including

(1) A conventional aft tail,

(2) A free-floating canard,

(3) A fixed canard,

(4) A geared canard driven in proportion to α for artificial stability, and

(5) A combination of canard and conventional tail.

The effectiveness of the tails for providing trim and stability was examined for conditions corresponding to those obtained for the model with a trailing-edge-flap deflection of 30° and a value of T_c' of 0.4 near $\alpha = 0^{\circ}$. (See fig. 11.) The analysis was conducted by using the equations presented in reference 7 and required the configuration to provide longitudinal trim, a 3-percent static margin, and a trimmed lift coefficient of 0.7. For analysis purposes, the conventional tail and canard were assumed to have lift-curve slopes of 0.06 per degree, nondimensional tail lengths of 1.0, and downwash factors $1 - \dfrac{d\epsilon}{d\alpha}$ of 0.5 and 1.0, respectively. For the geared canard, a lift-curve slope of -0.06 per degree was assumed, corresponding to a canard gear ratio $\dfrac{\Delta i_c}{\Delta \alpha} = -2.0$. A range of tail or canard area ratios S_t/S from 0 to 0.10 was evaluated; and the center-of-gravity position was allowed to vary in order to maintain a constant level of static margin as the tail area increased. The results of the study are presented in figure 17 in terms of the tail lift coefficient $C_{L,t}$ required for the range of S_t/S.

The data of figure 17(a) show that the conventional tail tested in this investigation $\left(S_t/S = 0.058\right)$ would require a lift coefficient of about 1.8 to provide trim and a static margin of 0.03. A tail lift coefficient of 1.8 should be achievable with high-lift devices; however, additional control is required for normal flight operations, and a larger

8

conventional tail would therefore be required. Increasing the size of a conventional tail has the advantage of shifting the neutral point of the configuration rearward to reduce the flap diving moment, but the conventional tail arrangement has the disadvantage of downward tail lift for trim which reduces the total lift of the airplane. In contrast to this condition, the fixed canard has the advantage of lifting upward for trim which increases the total lift, but it has the disadvantage of shifting the neutral point of the configuration forward. This forward shift in neutral point requires a forward shift in center of gravity (in order to maintain stability) which results in an increase in flap diving moments. One means of achieving the lift benefit of the canard without its destabilizing effect is to have the canard free floating (or have the canard mechanically driven so that its incidence angle does not change as the airplane angle of attack changes). Another approach would be to drive the canard surface so that its incidence angle is reduced as the airplane angle of attack is increased. This technique produces the benefits of both the canard and the conventional tail; that is, an upward lift for trim and a rearward shift in the neutral point for reduced flap diving moments and increased stability. Figure 17(a) shows that such an arrangement can reduce appreciably the canard lift coefficient required for trim. In addition, it is possible to reduce the size of this type of canard arrangement when the canard is combined with a conventional horizontal tail. In this combination, the conventional tail would operate at zero lift, or near zero lift, in low-speed flight.

The results presented in figure 17(a) were determined on the basis that the configuration must maintain a static margin of 0.03 for all conditions. Under this assumption, it was necessary to shift the center of gravity as the tail or canard size was changed in order to keep the static margin constant. Figure 17(b) illustrates the center-of-gravity variation as a function of S_t/S for each trim device investigated. The most significant point to be made regarding figure 17(b) is that the fixed or free-floating canard required a center-of-gravity location for low-speed flight forward of that required for supersonic-cruise flight and created a balance problem between the two speed ranges. In contrast, the conventional tail, the geared canard, or the combination of a geared canard with a conventional tail permit the configuration to be balanced at a center-of-gravity range consistent with that for supersonic-cruise flight. In particular, the geared canard (alone or in combination with a more conventional tail) gives the desired low-speed center-of-gravity range with very small canard surfaces. From the results of figures 17(a) and 17(b), it is concluded that an all-movable $\left(S_t/S \approx 0.02\right)$ canard in combination with a relatively small $\left(S_t/S \approx 0.07\right)$ conventional tail would provide an efficient means of achieving stability and trim in low-speed flight for the USB arrow-wing supersonic transport configuration of the subject tests.

It is recognized that alternate approaches to the stability and trim problem are available, such as fuel management and relaxed static stability, and a comprehensive study

beyond the scope of this paper is required to resolve the trade-offs and advantages of the various systems.

Performance comparison.- In order to better show the relative performance of the model with exhaust deflectors off and on, the lift-drag polars for the model with several flap settings have been replotted in figure 18. For purposes of comparison, a 3° descent angle, a 3° climb angle, and an $\alpha = 10^O$ ground-scrape angle are shown in each drag polar. On the assumption that the ratio of thrust coefficient to lift coefficient is equal to the ratio of thrust to weight (T/W), values of T/W for the 3° climb and descent conditions were determined from figure 18 and presented in figure 19 as plots of T/W against C_L. Also shown in figure 19 is the ground-scrape angle (10°) to help in establishing performance limits. It should be noted that for the data of figures 18 and 19, it was assumed that pitch trim could be achieved without penalizing the lift of the configuration. This assumption is based on the results of analysis presented in figure 17.

From the data of figure 19(a), it is seen that the maximum available lift coefficient for the model without deflectors is limited mostly by the ground-scrape angle and that the climb condition is much more critical than the glide condition in terms of the installed T/W ratio which is likely to be no greater than about 0.3 for a four-engine transport. The lift coefficient for the 3° climb condition is seen to increase from 0.50 up to about 0.73 by increasing the flap angle from 0° to 20° and by increasing the T/W ratio from 0.2 to 0.29. The 3° glide condition is seen to be limited to a lift coefficient of 0.68 for the 20° flap condition because of the ground-scrape angle.

A comparison of the data of figures 19(a) and 19(b) shows that the use of exhaust deflectors increased the lift coefficient at which the 10° ground-scrape angle occurred, but that higher values of T/W ratios are required to achieve the higher lift coefficients. Since the maximum installed T/W ratio is likely to be no greater than about 0.3, it is seen that the climb lift coefficients produced by upper-surface blowing would be limited to about 0.75 or 0.80. For the approach condition, the data of figure 19(b) show an available lift coefficient of about 0.92 for the 30° flap configuration at the ground-scrape angle and a value of T/W of only about 0.22. This condition suggests that higher flap angles could be utilized to increase the available approach lift coefficient without requiring excessively high values of T/W.

Lateral-Directional Characteristics

Lateral-stability characteristics measured at sideslip angles of $\pm 5^O$ for the model with trailing-edge flaps at 30° and for various thrust coefficients are presented for the tail-off and tail-on configurations in figures 20(a) and 20(b), respectively. Figure 20(a) shows that the model with tail off was slightly directionally stable $\left(C_{n_\beta}\right)$ at negative angles of attack but became directionally unstable $\left(-C_{n_\beta}\right)$ at the higher angles of attack. This

10

result is very different from that found in previous investigations of arrow-wing configurations in which it was found that the directional stability for the tail-off condition increased with increasing angle of attack. (For example, see ref. 6.) This previous result was attributed to the fact that in a sideslipped condition, the vortex flow from the leading wing produced a reversal of sidewash over most of the fuselage forward of the center of gravity. This sidewash produced a restoring yawing moment which made the configuration directionally stable. The fact that the present arrow-wing model with tail off was directionally unstable instead of stable probably results from flow interference between the wing and engines so that the wing vortex pattern was drastically altered. The data of figure 20(a) also show that the effective dihedral is positive $\left(-C_{l_\beta}\right)$ and increased with increasing angle of attack to extremely large values near an angle of attack of 20°.

The data for the tail-on configuration (fig. 20(b)) show that the vertical tail provided essentially a constant increment to directional stability for angles of attack up to about 20° and that the effective dihedral for the tail-on configuration was generally similar to that for the tail-off configuration. In general, the effects of thrust on the lateral-directional stability were relatively small.

Lateral control characteristics.- Presented in figure 21 are the lateral forces and moments produced by spoiler deflection. The spoiler was located aft of the left engine at a position directly forward of the inboard flap. (See fig. 2.) The data show that relatively large rolling and yawing moments were produced by spoiler deflection, and indicated that the spoiler may be an effective lateral-control device in the propulsive-lift system for supersonic transport. The spoiler may also be useful for roll trim for the engine-out condition although the lift data of figure 21(b) show that the lift losses associated with 60° of spoiler deflection were very large.

Engine-out characteristics.- The problem of engine-out lateral trim can be very severe in a propulsive-lift system. To provide some fundamental information on the engine-out lateral problem of the present model, tests were conducted with the left engine inoperative and the results are presented in figure 22. Because in a powered-lift system a partial loss of engine power results in loss of lift, plots of the lateral characteristics with one engine inoperative are accompanied by plots of the corresponding longitudinal characteristics.

The data of figure 22(a) show that, as expected, large yawing and rolling moments were generated with an engine inoperative. The engine-out (windmilling) moments generally showed an increase with increasing angle of attack. Observation of tuft flow pattern on the upper surface of the model indicated that the engine-out wing tended to stall first. Comparison of the corresponding lift data (fig. 22(b)) with lift data for symmetrical thrust (fig. 10) shows that large losses in lift also occur with engine failure.

Presented in figures 23 and 24 are the results of tests to study the use of asymmetric BLC over the flap of the engine-out wing as a means of providing roll trim. The data of figure 23 were obtained with blowing on the most inboard flap segment only; whereas, the data of figure 24 were obtained with blowing over both the two inboard flap segments. (See fig. 2(c).) The data of figures 23 and 24 show that engine-out roll trim could be achieved up to moderate angles of attack with asymmetric blowing, but that excessively high values of C_μ were required.

The foregoing considerations illustrate the severity of the engine-out problem for a two-engine upper-surface blowing configuration. However, it should be noted that with a four-engine configuration, the loss of engine power on a single engine would result in a reduction of total thrust of only 25 percent, as compared with the 50-percent thrust reduction previously considered. In order to establish the relative magnitude of the engine-out problem for a four-engine USB configuration (Siamese pod), tests were conducted for the left engine operating at one-half the thrust of the right engine. The results of these tests as presented in figure 25 show that the engine-out rolling moment associated with a four-engine USB configuration would be about 75 percent of the engine-out rolling moment associated with a two-engine USB.

SUMMARY OF RESULTS

Force tests of a large-scale advanced arrow-wing supersonic transport with engines mounted above the wing for upper-surface blowing show the following results:

1. The upper-surface blowing concept was effective for providing increased lift for improved take-off and landing performance.

2. Large diving moments accompanied high propulsive lift. However, the analysis indicates that an all-movable canard in combination with a relatively small conventional tail may be an effective arrangement for achieving longitudinal stability and trim at high lift.

3. The model with tail on exhibited static directional stability up to an angle of attack of about 20° and had high positive effective dihedral.

4. Spoiler deflection provided relatively large lateral control moments.

5. Large rolling and yawing moments were introduced with one engine inoperative. The use of asymmetric boundary-layer control (BLC) on the trailing-edge flaps achieved roll trim for moderate angles of attack but excessively high values of flow coefficient were required.

6. The available approach lift coefficient can be increased by use of large flap angle deflection in conjunction with exhaust nozzle deflectors without requiring excessively high values of thrust-weight ratio.

Langley Research Center
National Aeronautics and Space Administration
Hampton, VA 23665
October 5, 1976

REFERENCES

1. McLemore, H. Clyde; Parlett, Lysle P.; and Sewall, William G.: Low-Speed Wind-Tunnel Tests of a 1/9-Scale Model of a Variable-Sweep Advanced Supersonic Transport. NASA TM X-71960, 1974.

2. McLemore, H. Clyde; and Parlett, Lysle P.: Low-Speed Wind-Tunnel Tests of a 1/10-Scale Model of a Blended-Arrow Advanced Supersonic Transport. NASA TM X-72671, 1975.

3. Morris, Odell A.; and Fournier, Roger H.: Aerodynamic Characteristics at Mach Numbers 2.30, 2.60, and 2.96 of a Supersonic Transport Model Having a Fixed, Warped Wing. NASA TM X-1115, 1965.

4. Morris, Odell A.; and Patterson, James C., Jr.: Transonic Aerodynamic Characteristics of a Supersonic Transport Model With a Fixed, Warped Wing Having 74° Sweep. NASA TM X-1167, 1965.

5. Heyson, Harry H.: Use of Superposition in Digital Computers To Obtain Wind-Tunnel Interference Factors for Arbitrary Configurations, With Particular Reference to V/STOL Models. NASA TR R-302, 1969.

6. Freeman, Delma C., Jr.: Low Subsonic Flight and Force Investigation of a Supersonic Transport Model With a Highly Swept Arrow Wing. NASA TN D-3887, 1967.

7. Johnson, Joseph L., Jr.: Wind-Tunnel Investigation of the Static Longitudinal Stability and Trim Characteristics of a Sweptback-Wing Jet-Transport Model Equipped With an External-Flow Jet-Augmented Flap. NACA TN 4177, 1958.

TABLE I.- DIMENSIONAL CHARACTERISTICS OF MODEL

Wing:
- Area, m^2 (ft^2) 10.232 (110.14)
- Span, m (ft) 4.191 (13.750)
- Aspect ratio 1.72
- Spanwise station of mean aerodynamic chord, m (ft) 0.642 (2.105)
- Incidence relative to horizontal reference line, deg . . . . -5.240
- Root chord, m (ft) 5.608 (18.399)
- Mean aerodynamic chord, m (ft) 3.368 (11.050)
- Tip chord, m (ft) 0.540 (1.772)
- Leading-edge sweep, deg (Body stations 49.87 and 187.31) 74.00
- Leading-edge sweep, deg (Body stations 187.31 and 247.38) 70.50
- Leading-edge sweep, deg (Body stations 247.38 and 286.64) 60.00

Vertical tail:
- Area, m^2 (ft^2) 0.823 (8.859)
- Span, m (ft) 0.760 (2.493)
- Sweep angle:
  - At leading edge, deg 37.00
  - At trailing edge, deg 30.00
- Root chord, m (ft) 1.900 (6.234)
- Tip chord, m (ft) 0.640 (2.100)

Vertical fin (two):
- Area, m^2 (ft^2) (Total) 0.415 (4.467)
- Span, m (ft) 0.328 (1.075)
- Aspect ratio (each) 0.517
- Sweep angle:
  - At leading edge, deg 73.40
  - At trailing edge, deg 16.40
- Root chord, m (ft) 1.109 (3.638)
- Tip chord, m (ft) 0.158 (0.518)

Horizontal tail:
- Area, m^2 (ft^2) 0.651 (7.197)
- Span, m (ft) 1.420 (4.667)
- Length of mean aerodynamic chord, m (ft) 0.500 (1.640)
- Leading-edge sweep angle, deg 45.00
- Root chord, m (ft) 0.700 (2.297)
- Tip chord, m (ft) 0.240 (0.792)
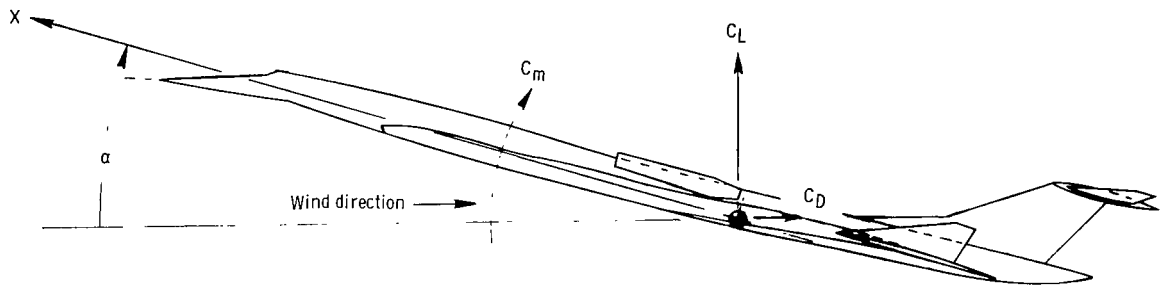
(a) Wind axis.
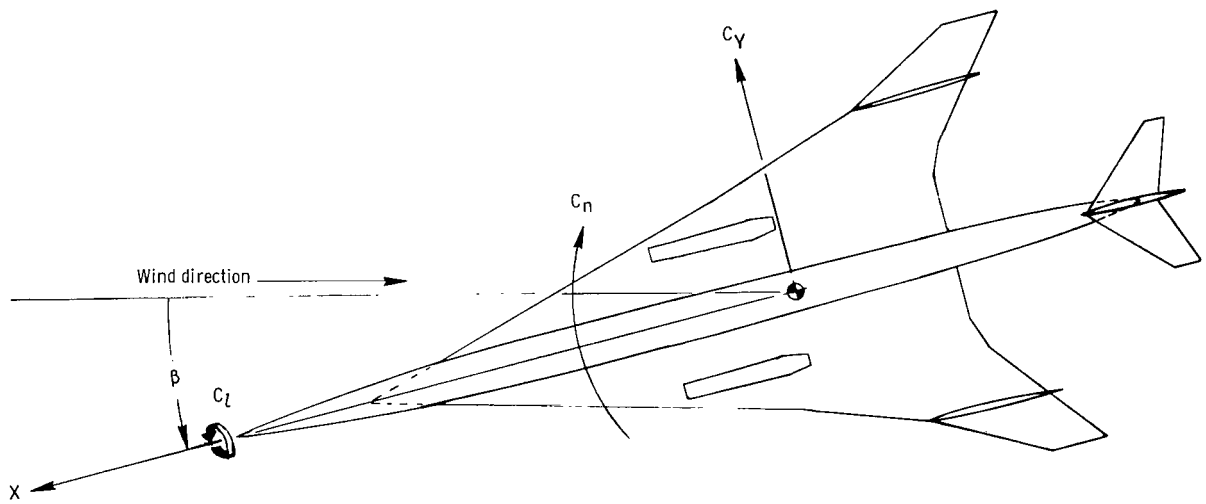
(b) Body axis.

Figure 1.- Axes systems.
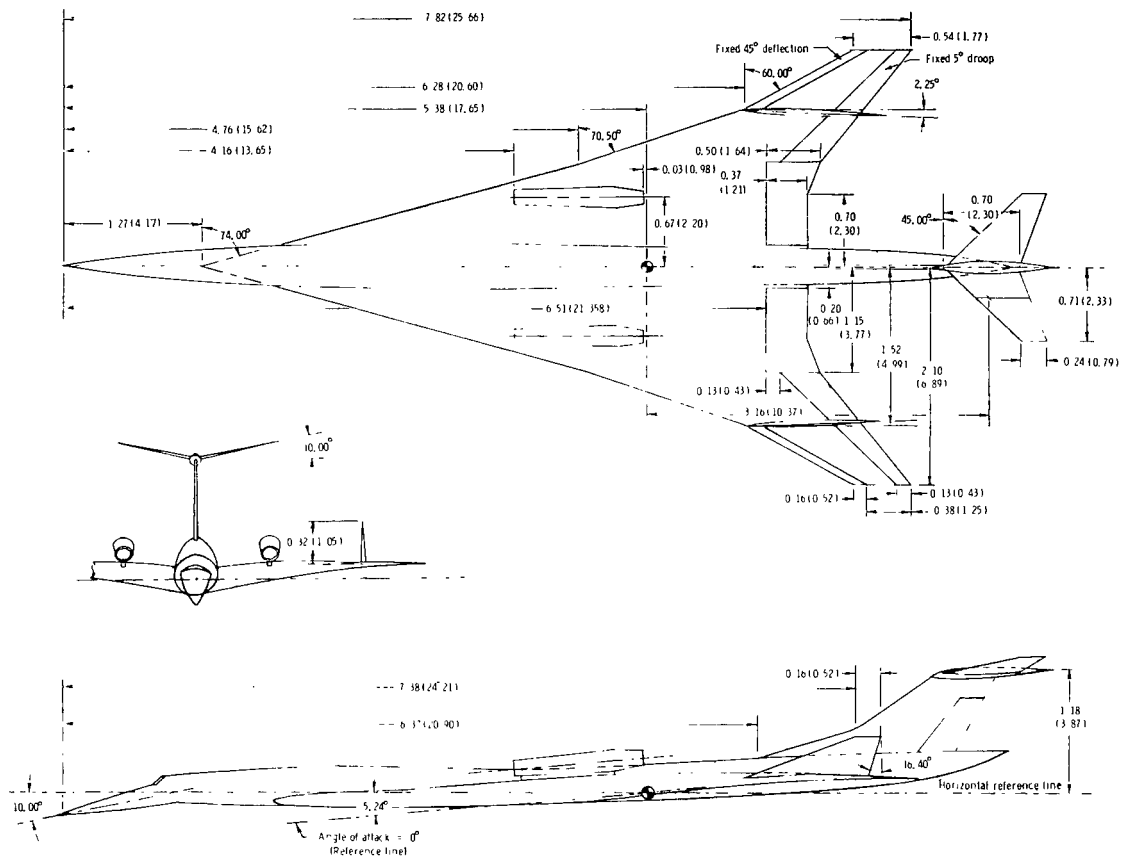
(a) Three-view drawing of model.

Figure 2.- Dimensional characteristics of model. Dimensions are in meters (ft). B.S. denotes body station.

B. S. 1.270 (4.167)

B. S. 3.566 (11.701)

B. S. 5.379 (17.646)

0.642 (2.105)

B. S. 6.934 (22.751)

c̄ = 3.368 (11.050)

B. S. 4.160 (13.647)
0.152D (0.500)

B. S. 5.101 (16.737)

B. S. 5.345 (17.535)

Compressed air-driven fan, 0.140D (0.458)

A

20°

0.213D (0.700)

0.132D (0.433)

2.25° toe out

B

0.067 (0.221)

Approximate wing surface

Enlarged view of engine with 20° eyelid exhaust deflector

0.305 (1.000)

0.055 (0.182)

0.016 (0.052)

0.430 (1.410)

B. S. 7.383 (24.223)

0.101 (0.333)

Body reference line
α = 0° reference line

0.158 (0.520)

0.387 (1.271)

73.4°

0.328 (1.075)

Fuselage

Section A-A
c = 3.216 (10.550)

c = 0.992 (3.255)

0.170 (0.558)

3.599 (11.807)

Section B-B

B. S. 6.279 (20.600)

(b) Geometric relationships at engine and fin stations.   All dimensions are in meters (ft).

Figure 2.- Continued.

Thin sheetmetal plenum welded to tube

Holes drilled in thin wall tube

To separate air controllers; BLC on left wing only

Spoiler set at 60° up relative to upper surface; chord length of 15.24 (6) cm (in.)

−0.020 slot gap (constant ± 0.002)

External air source

Rib supports equally spaced along plenum chamber

BLC plenum to each flap

Plenum cross-section sketch

Spoiler, plenum, flap combination sketch

(c) Sketch of flap boundary-layer control and spoiler installation.

Figure 2.- Concluded.
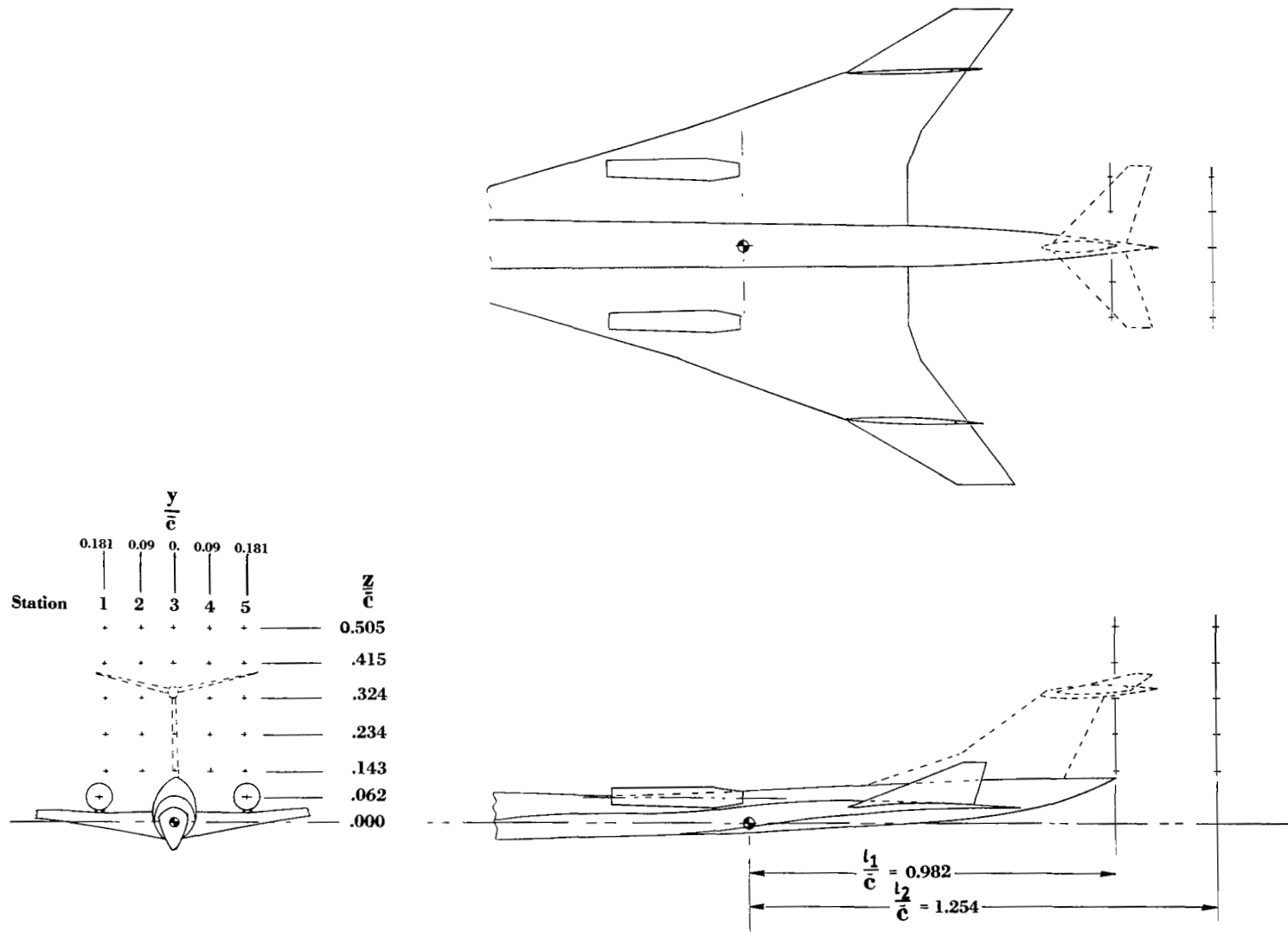
Figure 3.- Location of downwash survey rake positions for tail-off configuration.
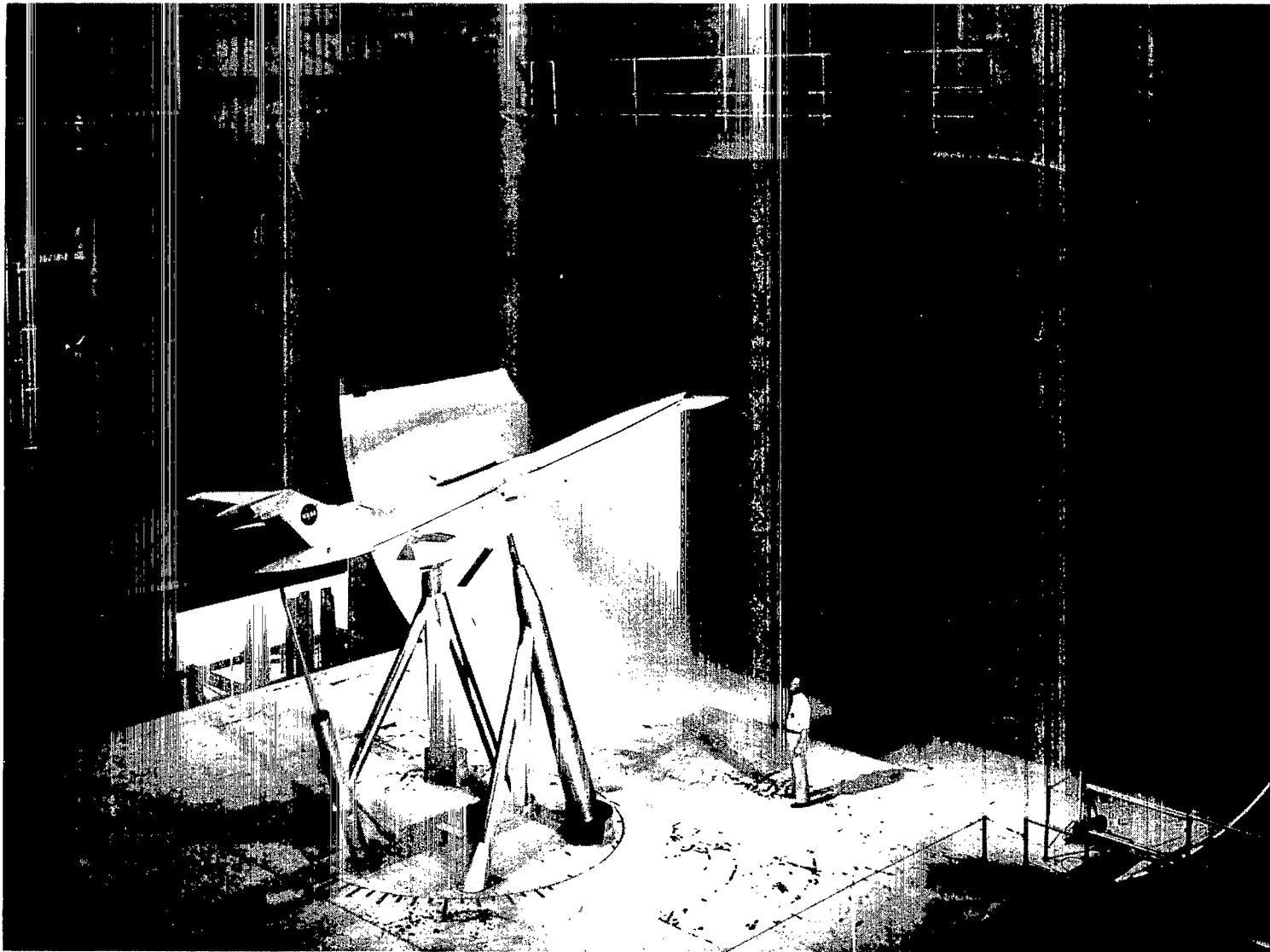
L-74-2729

Figure 4.- Three-quarter rear view of the model mounted for tests in the Langley full-scale tunnel.
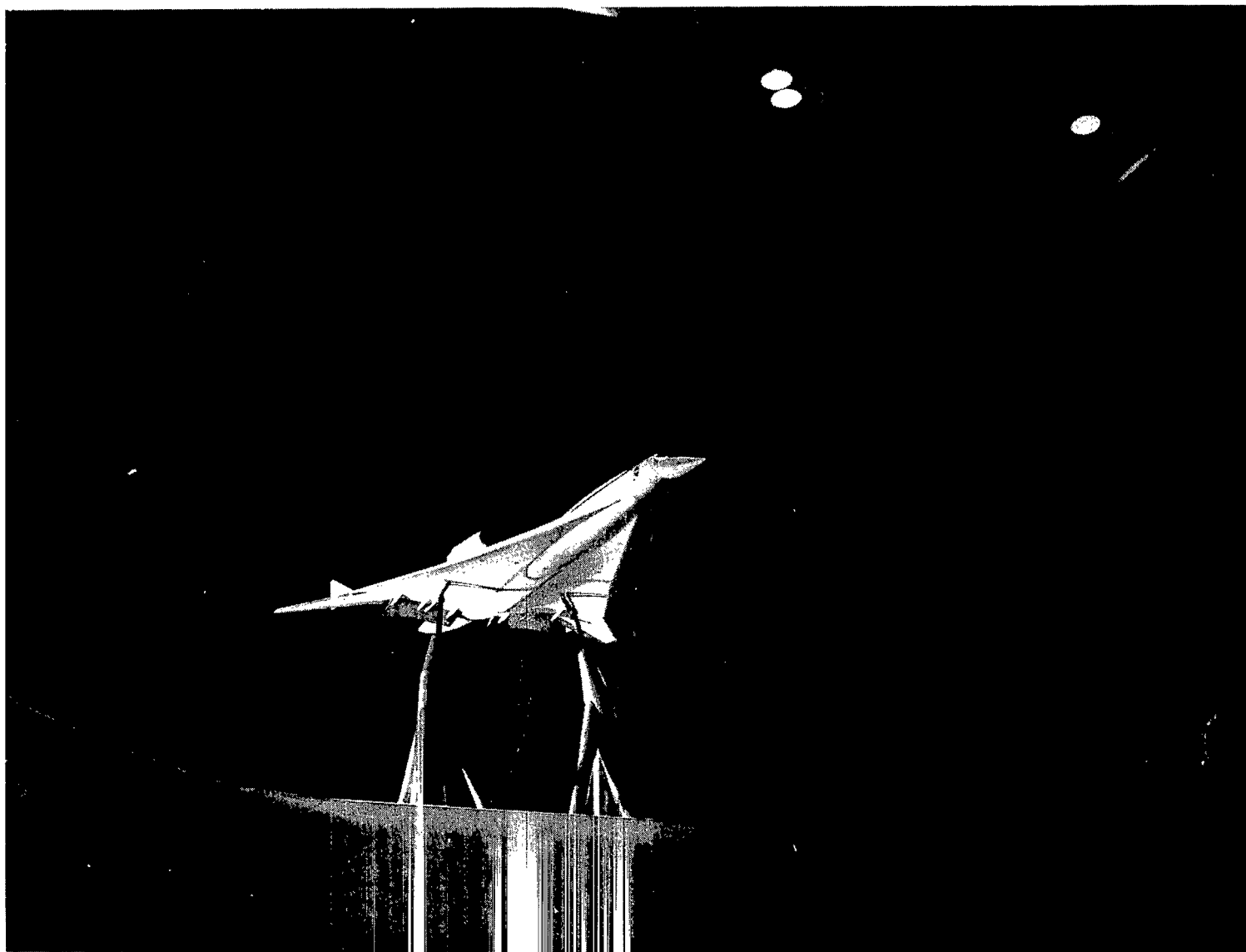
L-74-2564

Figure 5.- Three-quarter front view of the model mounted for tests in the Langley full-scale tunnel.

Figure 6.- Static turning performance.
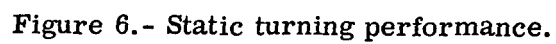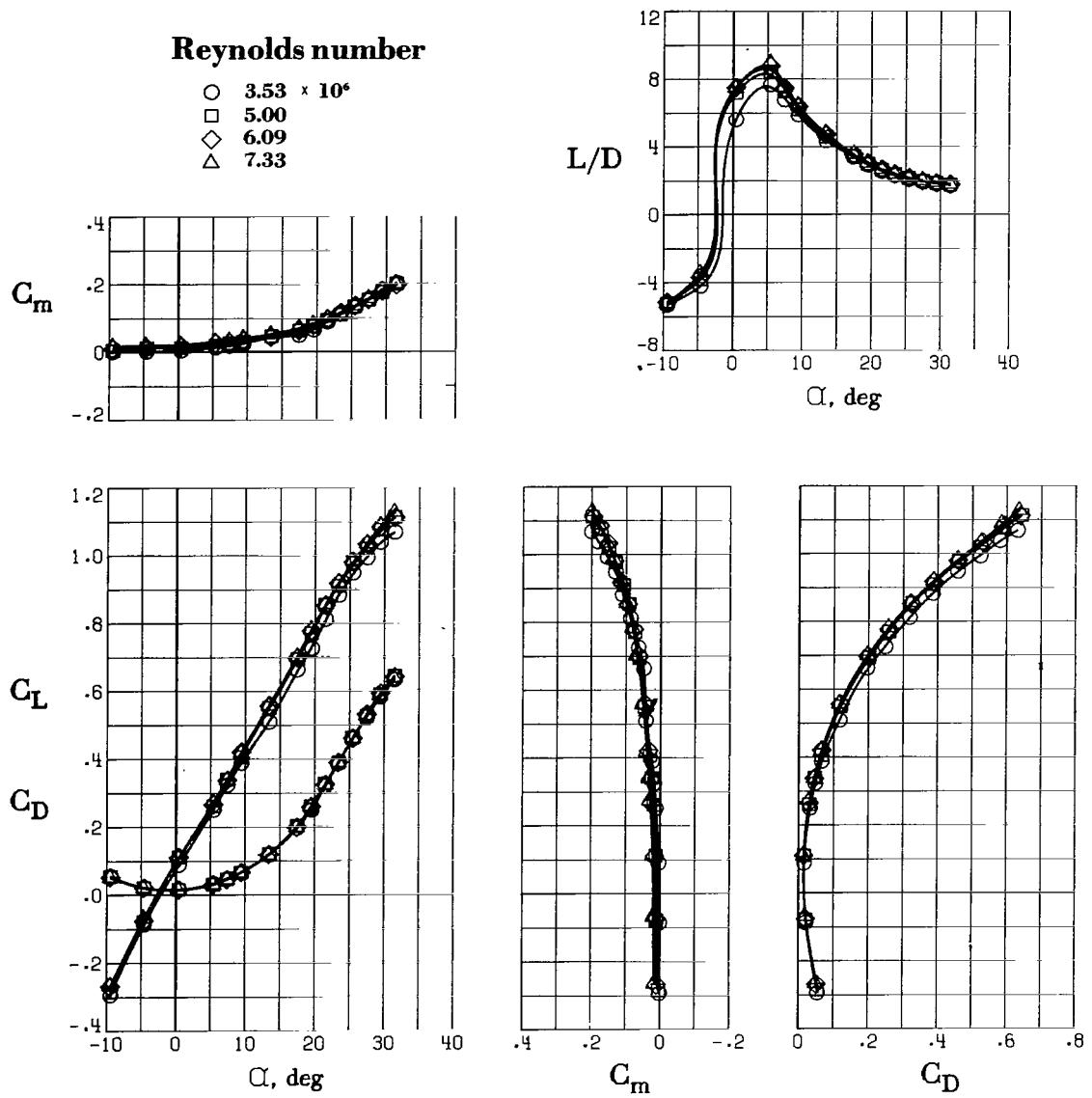
Figure 7.- Effect of Reynolds number on longitudinal aerodynamic characteristics. $\delta_f = 0^O$. $T_c' = 0$.

(a) $\delta_f = 0^o$.
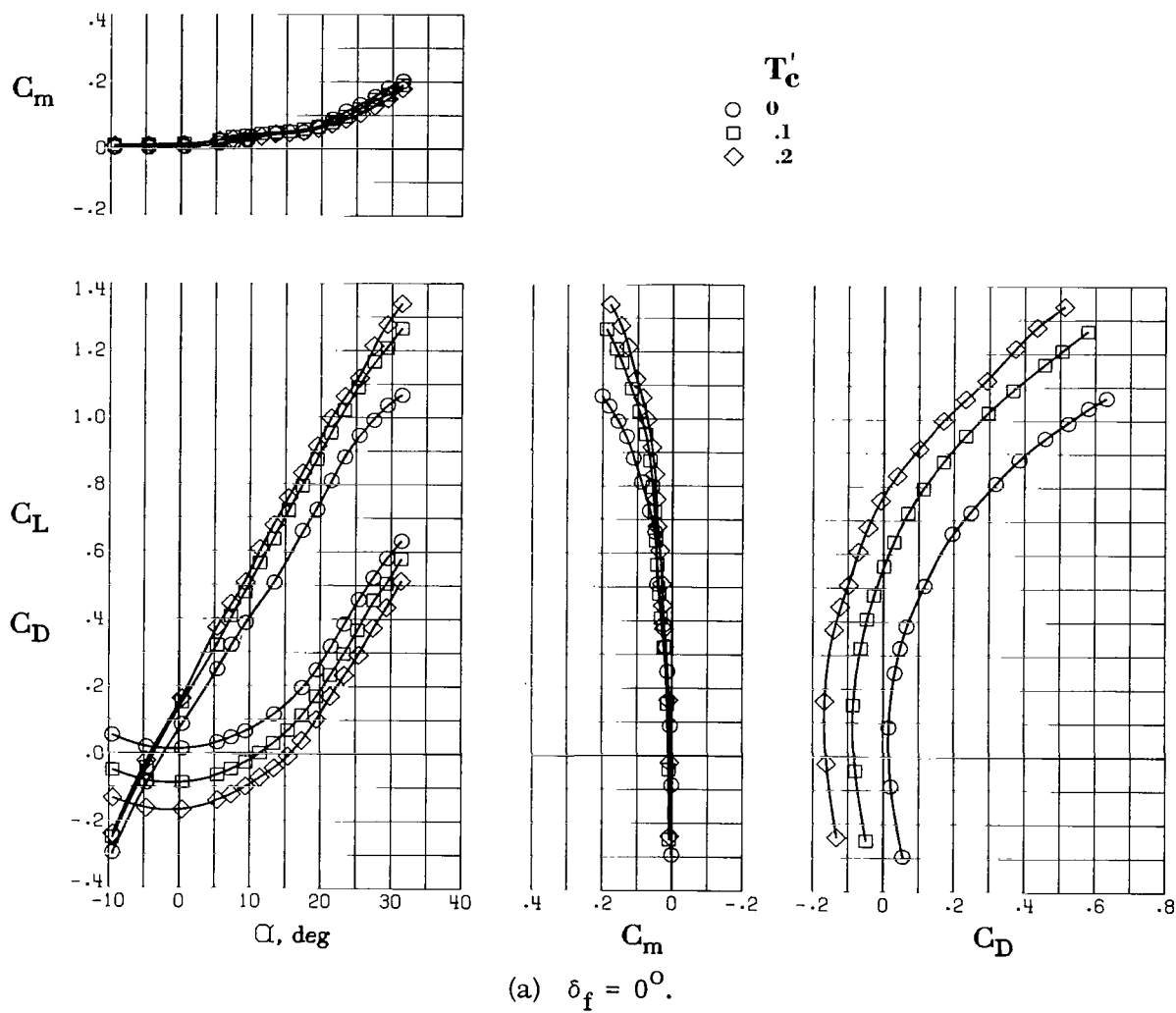
Figure 8.- Effect of thrust on longitudinal aerodynamic characteristics.
No exhaust deflectors on engines.

(b) $\delta_f = 10^{O}$.
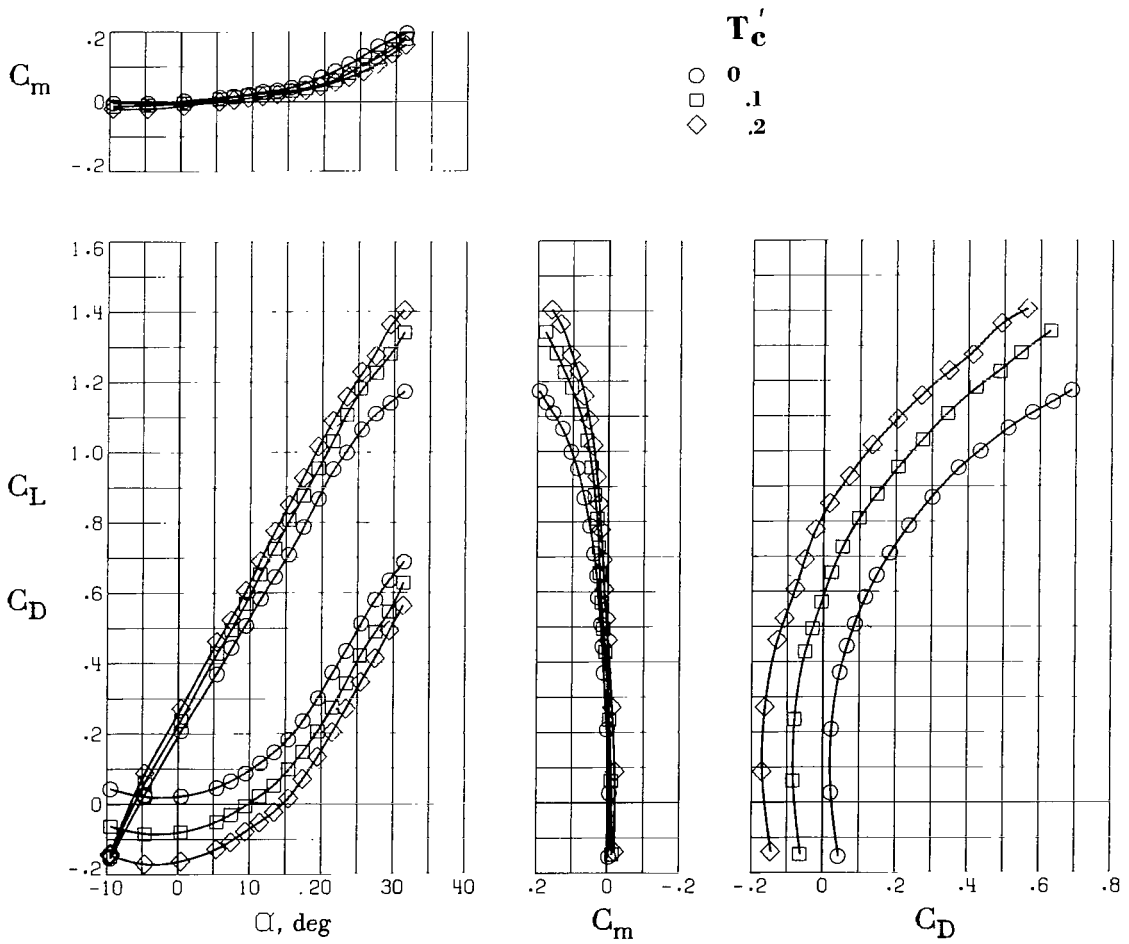
Figure 8.- Continued.

(c) $\delta_f = 20^o$.
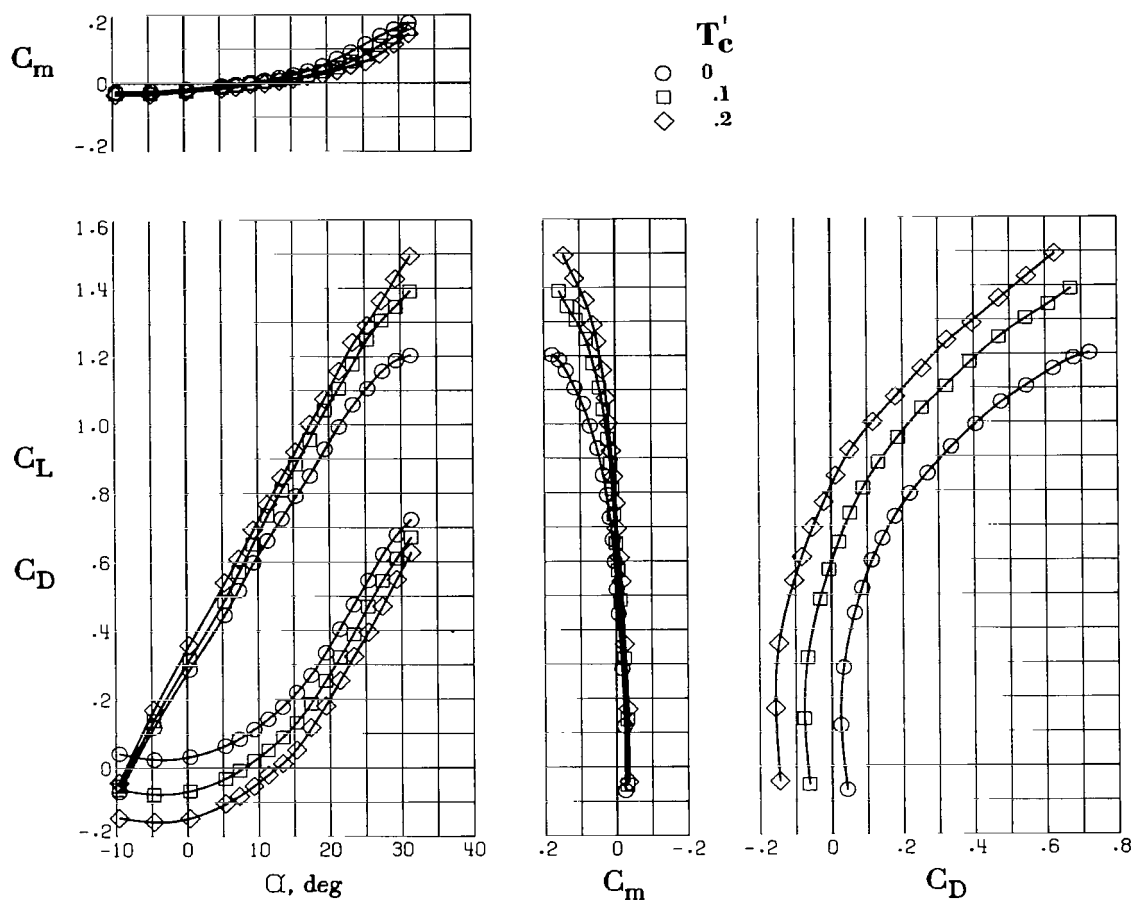
Figure 8.- Concluded.
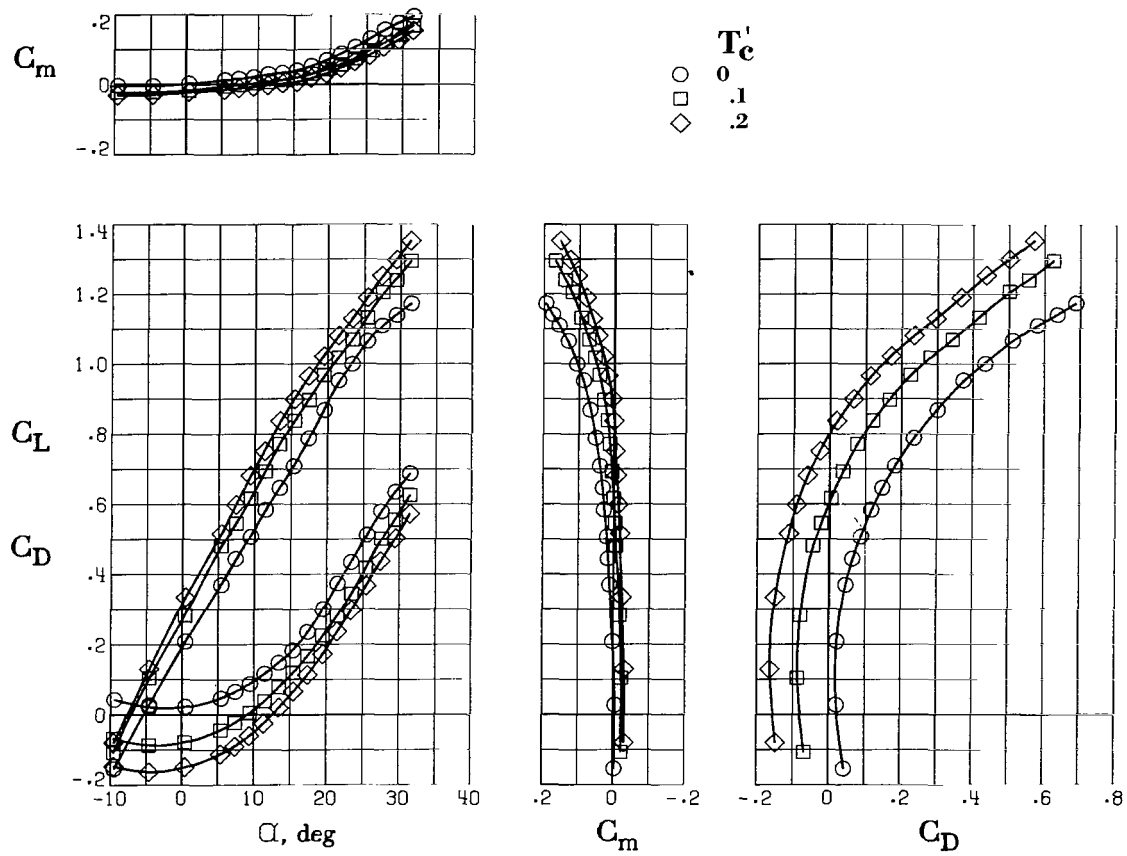
(a) 20° exhaust deflectors installed.

Figure 9.- Effect of thrust on longitudinal aerodynamic characteristics. $\delta_f = 10^O$.
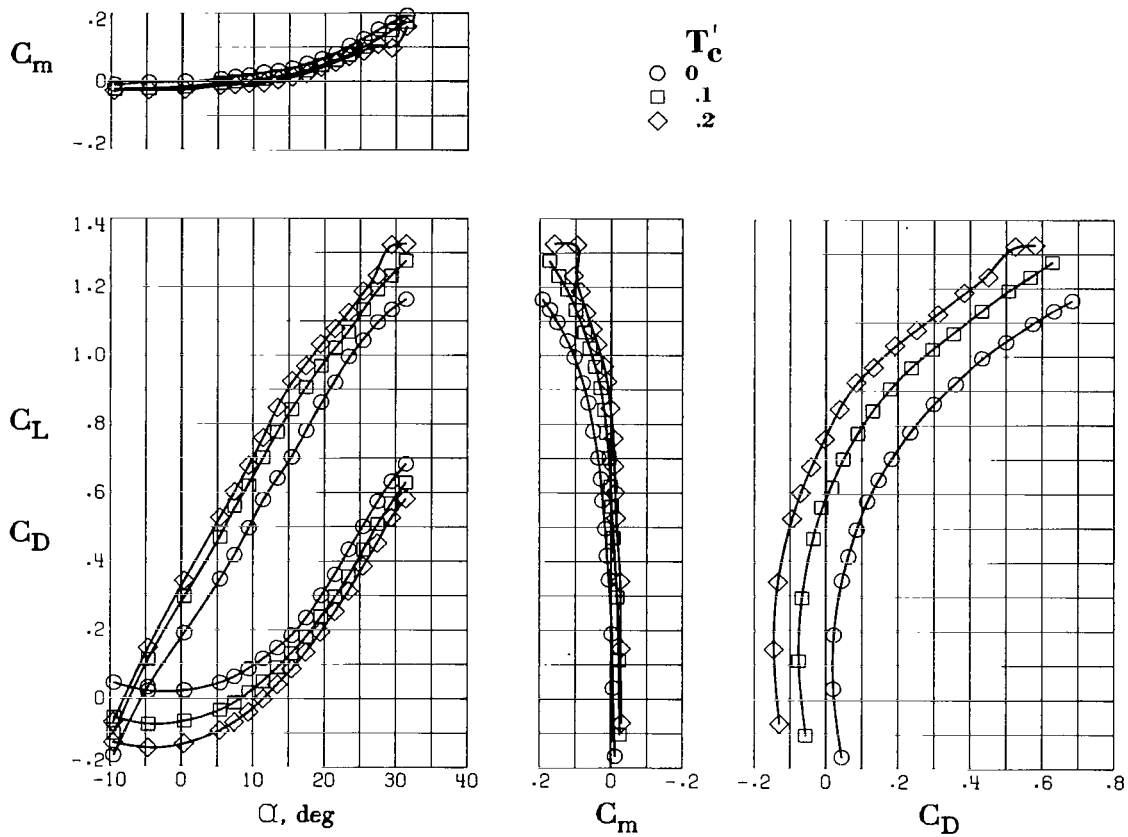
(b) 30° exhaust deflectors installed.

Figure 9.- Concluded.
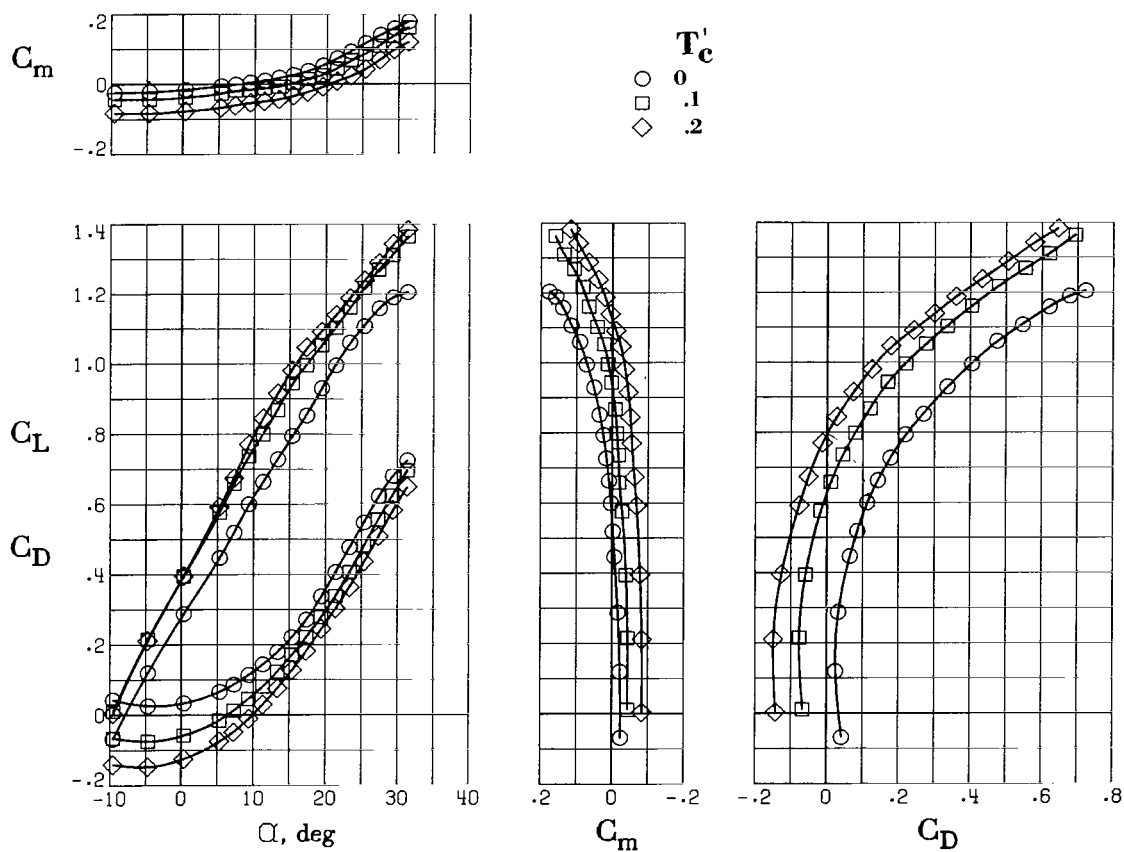
(a) 20° exhaust deflectors installed.

Figure 10.- Effect of thrust on longitudinal aerodynamic characteristics. $\delta_f = 20°$.
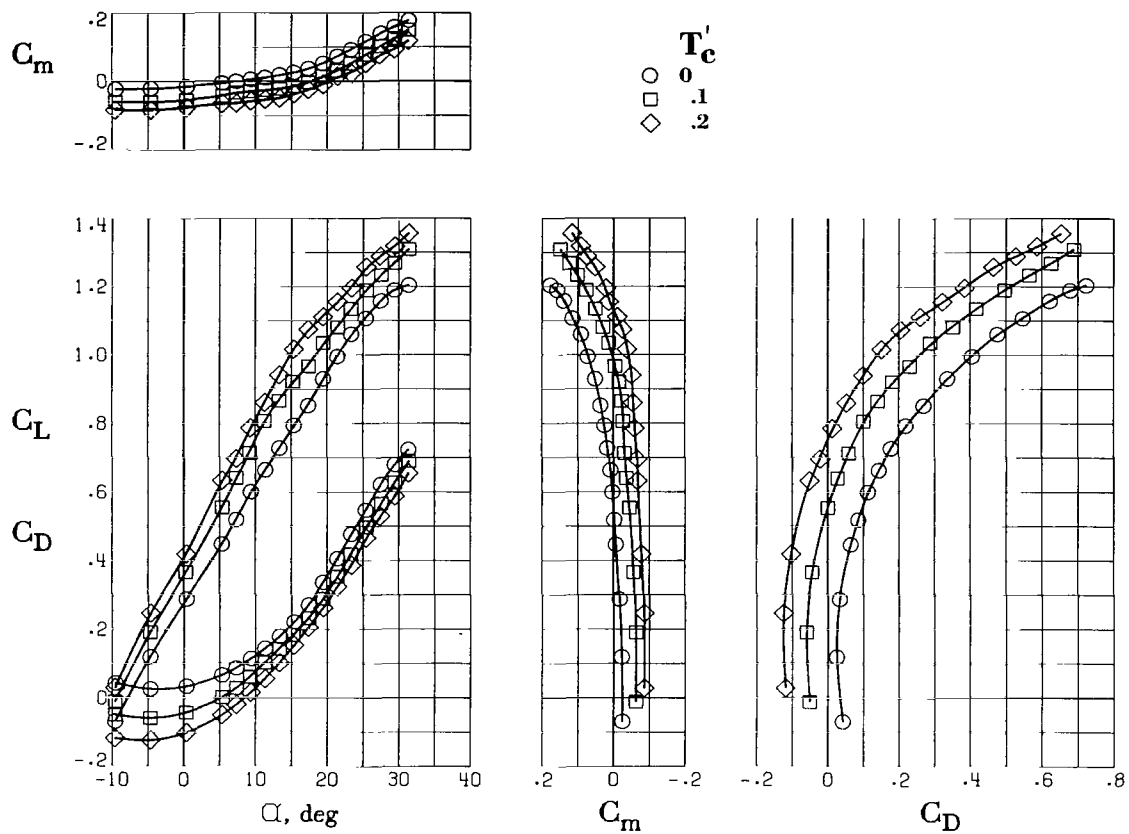
(b) 30° exhaust deflectors installed.

Figure 10.- Concluded.
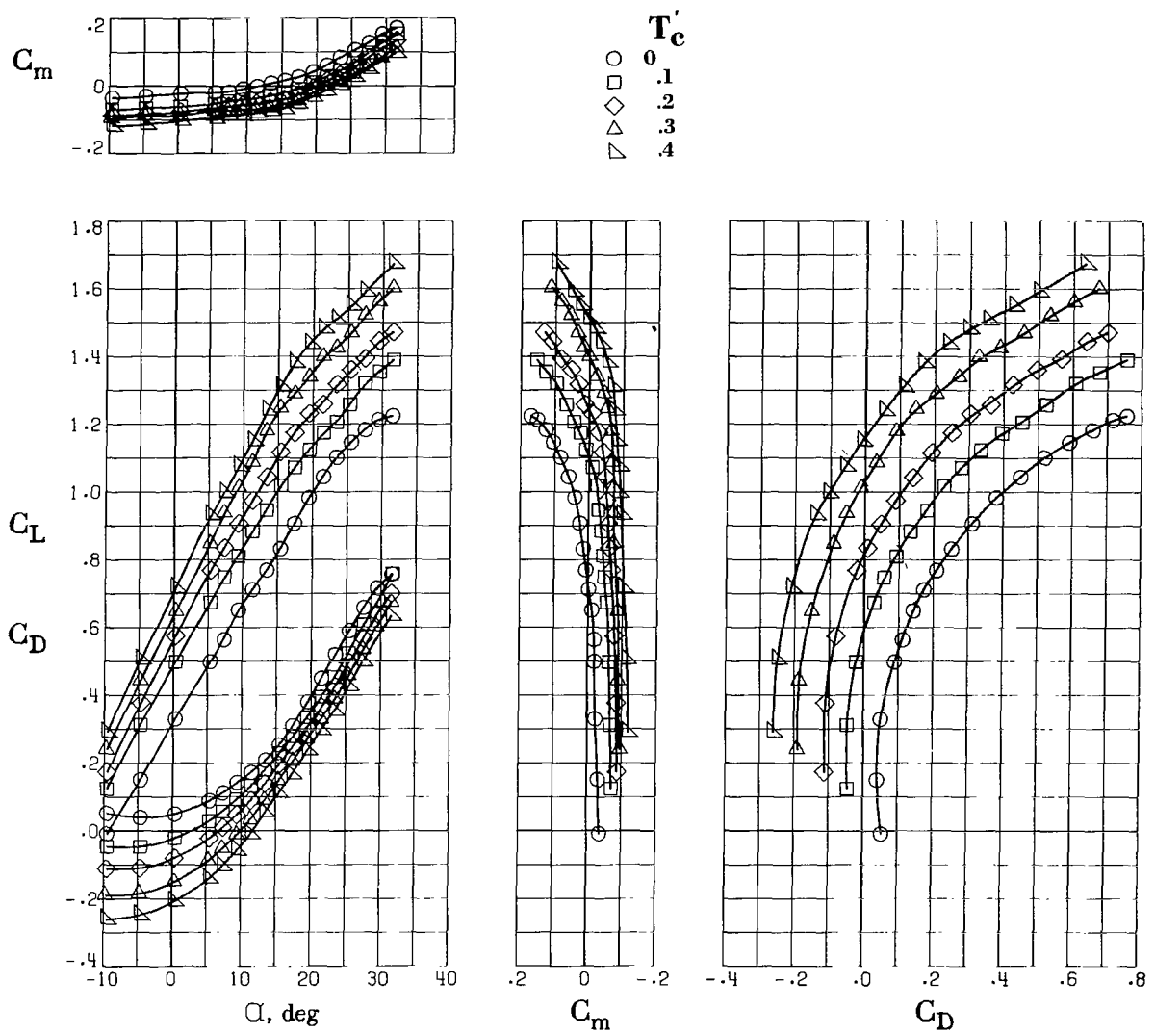
Figure 11.- Effect of thrust on longitudinal aerodynamic characteristics. $\delta_f = 30^O$. 20° exhaust deflectors installed.
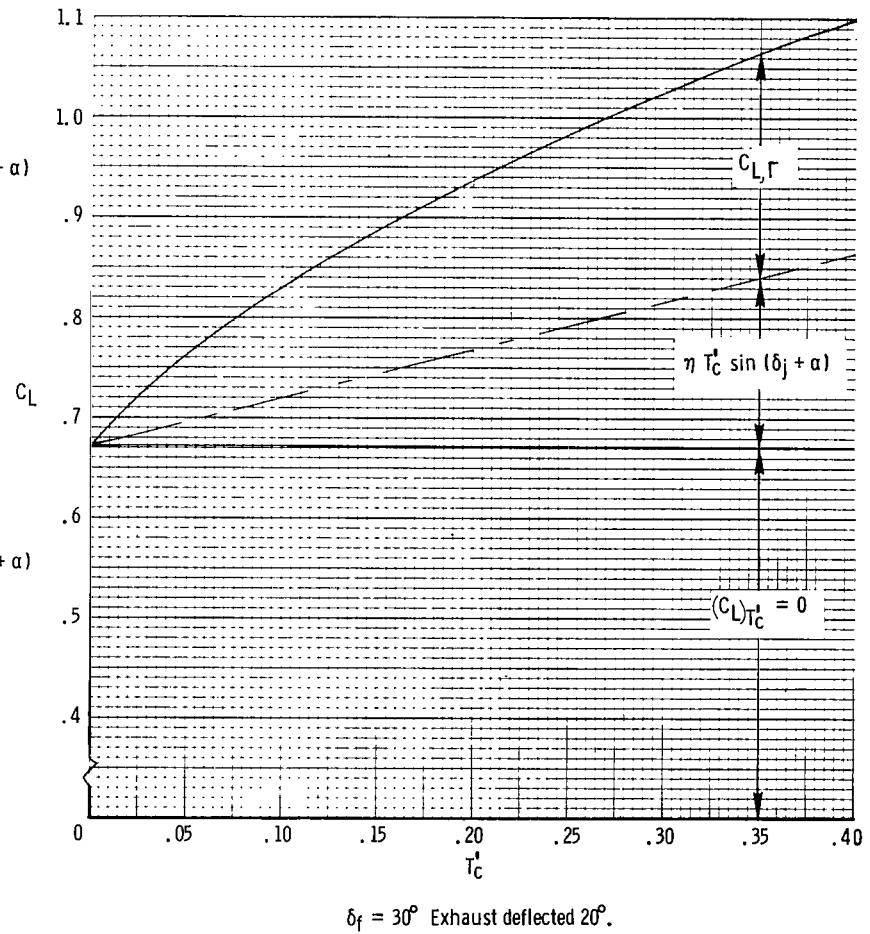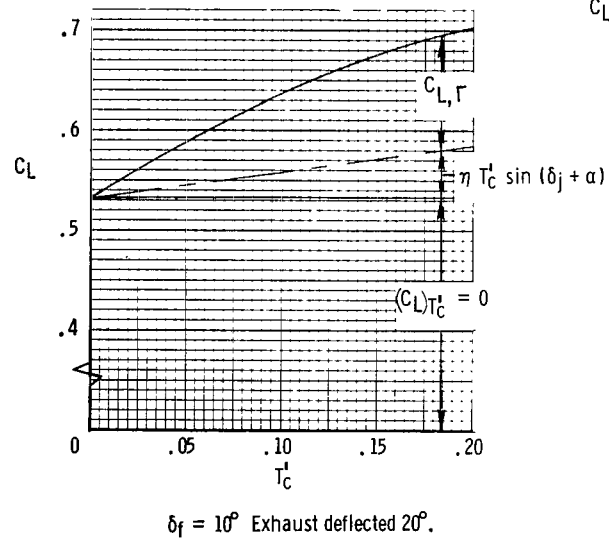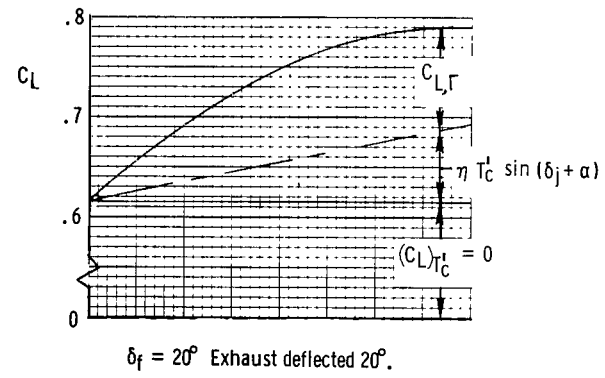
Figure 12.- Variation of lift components with thrust coefficient. $\alpha = 10^O$.
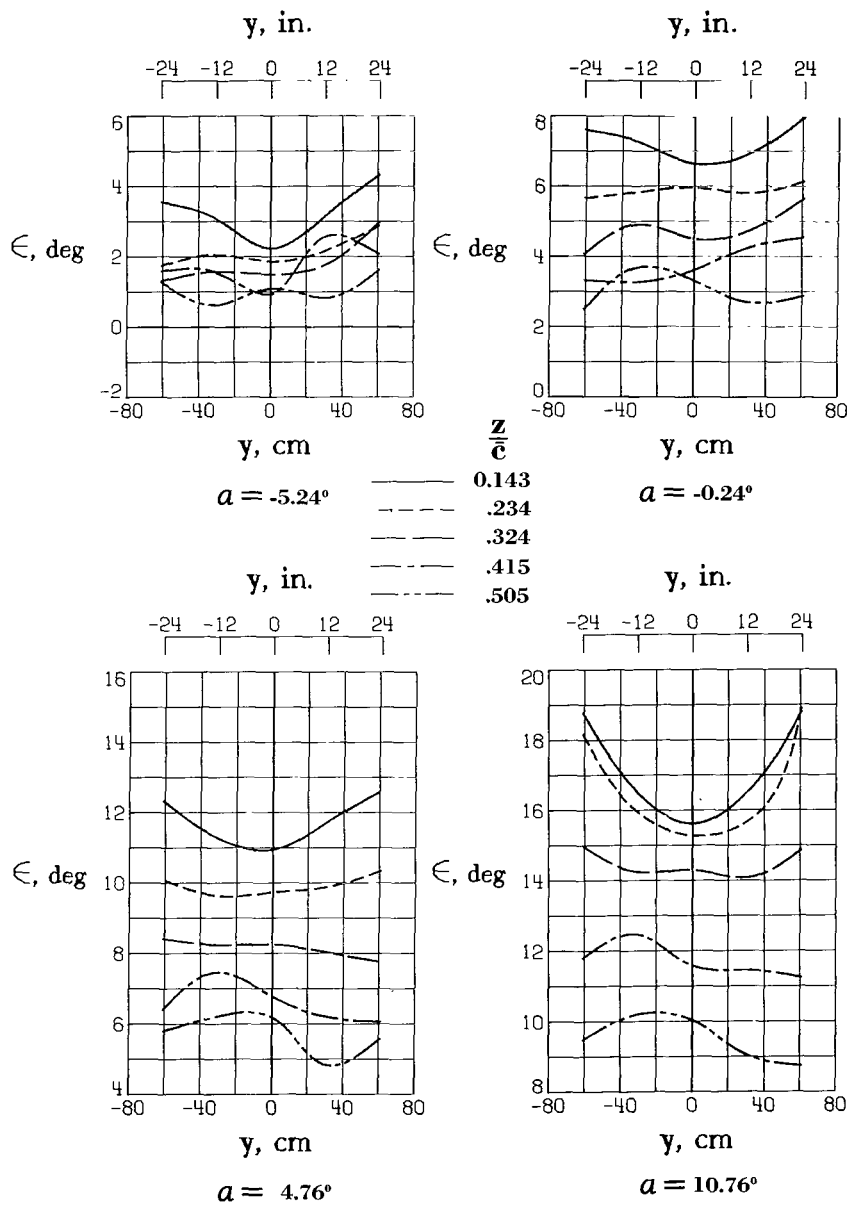
(a) $T_c' = 0$; $l/\bar{c} = 0.982$.

Figure 13.- Variation of downwash angle with spanwise station.
$\delta_f = 20^\circ$. Deflectors off.

y, in.

$\frac{z}{\bar{c}}$

——————— 0.143
— — — — — .234
— —— — —— .324
—·—— —·—— .415
—··——··— .505

$\in$, deg

$a = -0.24°$

y, cm

y, in.

$\in$, deg

y, cm

$a = 4.76°$

y, in.

$\in$, deg

y, cm

$a = 10.76°$
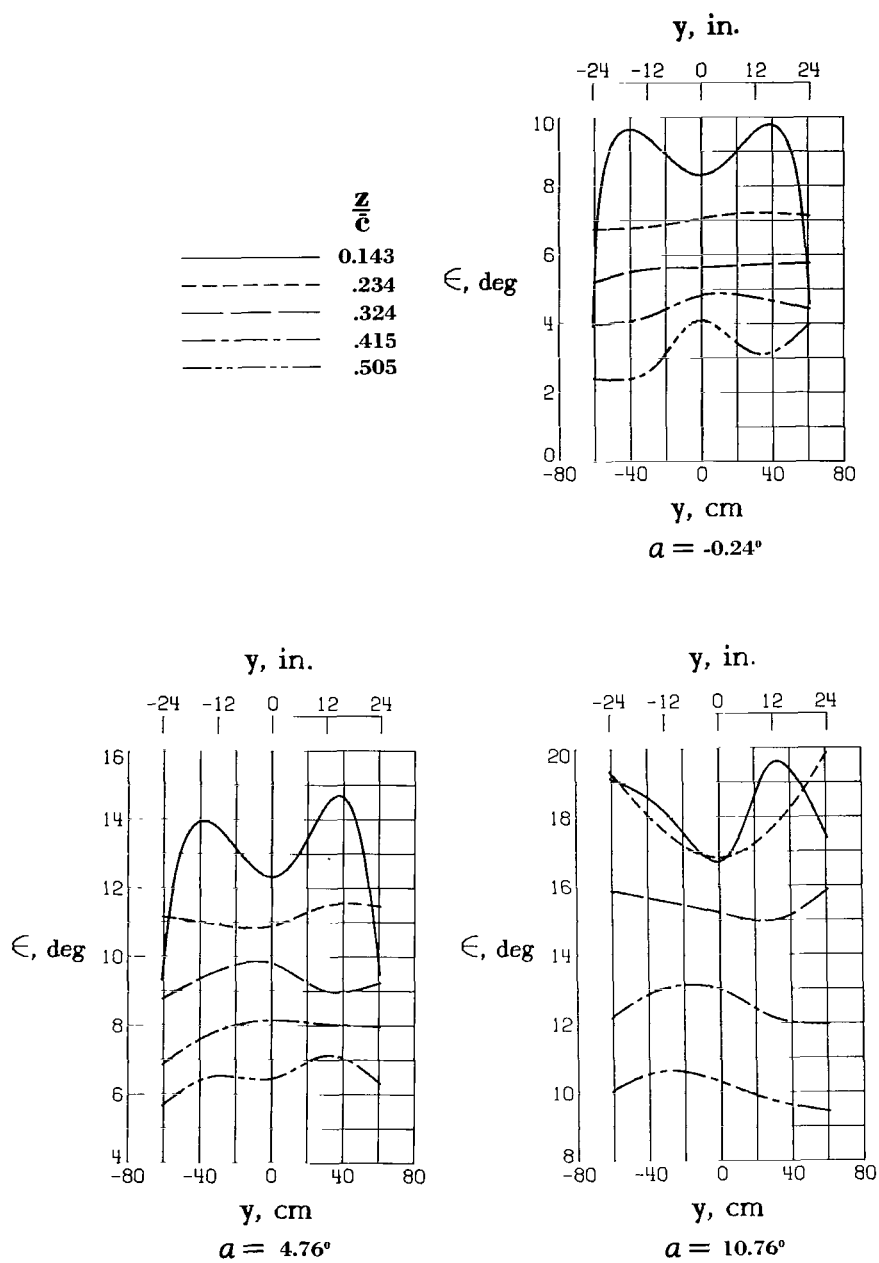
(b) $T_c{}' = 0.2$; $l/\bar{c} = 0.982$.

Figure 13.- Continued.

y, in.

-24 -12 0 12 24

6

4

ϵ, deg 2

0

-2

-80 -40 0 40 80

y, cm

$a = $ -5.24°

$\frac{z}{\bar{c}}$

———— 0.143

----- .234

— — .324

—·— .415

—··— .505

y, in.

-24 -12 0 12 24

10

8

ϵ, deg 6

4

2

-80 -40 0 40 80

y, cm

$a = $ -0.24°

y, in.

-24 -12 0 12 24

16

14

12

ϵ, deg 10

8

6

4

2

-80 -40 0 40 80

y, cm

$a = $ 4.76°

y, in.

-24 -12 0 12 24

22

20

18

ϵ, deg 16

14

12

10

8

-80 -40 0 40 80

y, cm

$a = $ 10.76°
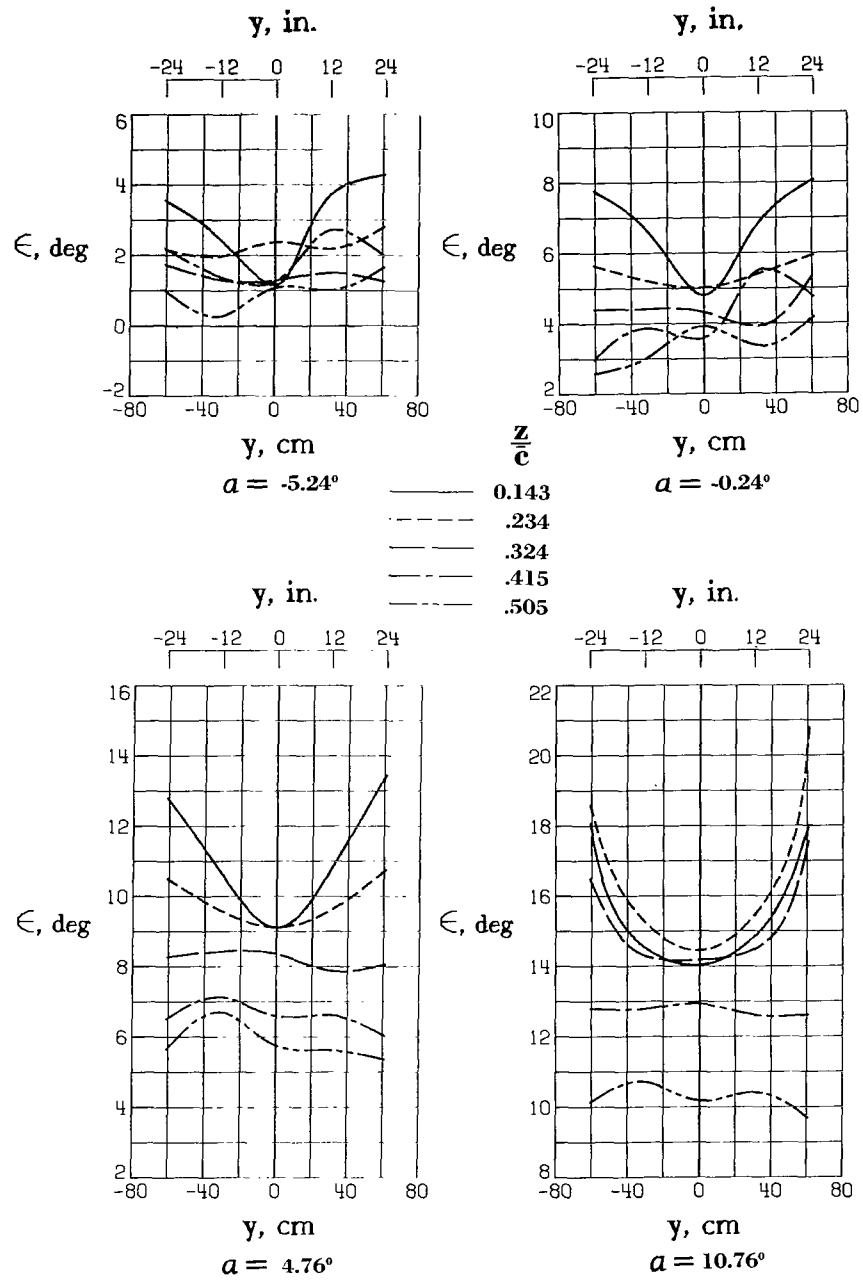
(c) $T_c' = 0$; $l/\bar{c} = 1.254$.

Figure 13.- Continued.

36

$\frac{z}{\bar{c}}$

$a = -0.24°$

$a = 4.76°$

$a = 10.76°$
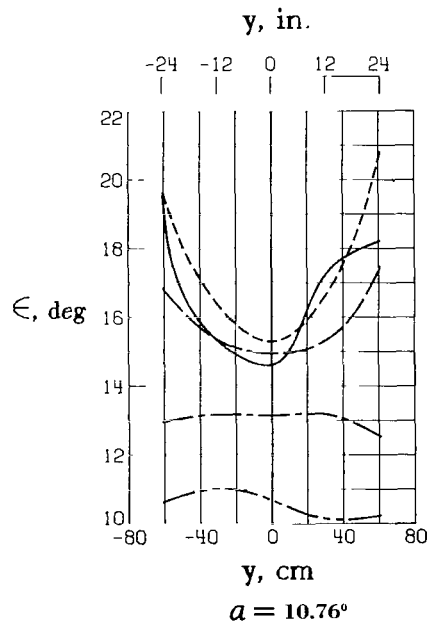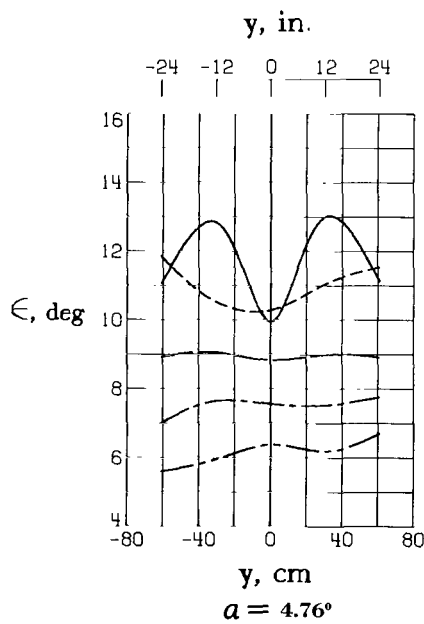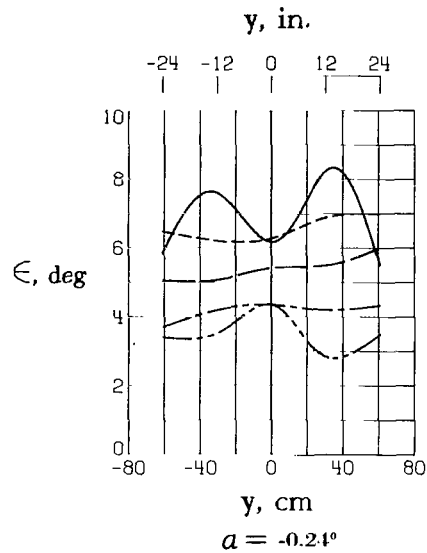
(d) $T_c' = 0.2;$ $l/\bar{c} = 1.254.$

Figure 13.- Concluded.

y, in.

€, deg

$a = -5.24°$

y, in.

€, deg

$a = -0.24°$

$\dfrac{z}{\bar{c}}$

——— 0.143
- - - - .234
— — .324
—·— .415
—··— .505

y, in.

€, deg

$a = 4.76°$

y, in.

€, deg

$a = 10.76°$
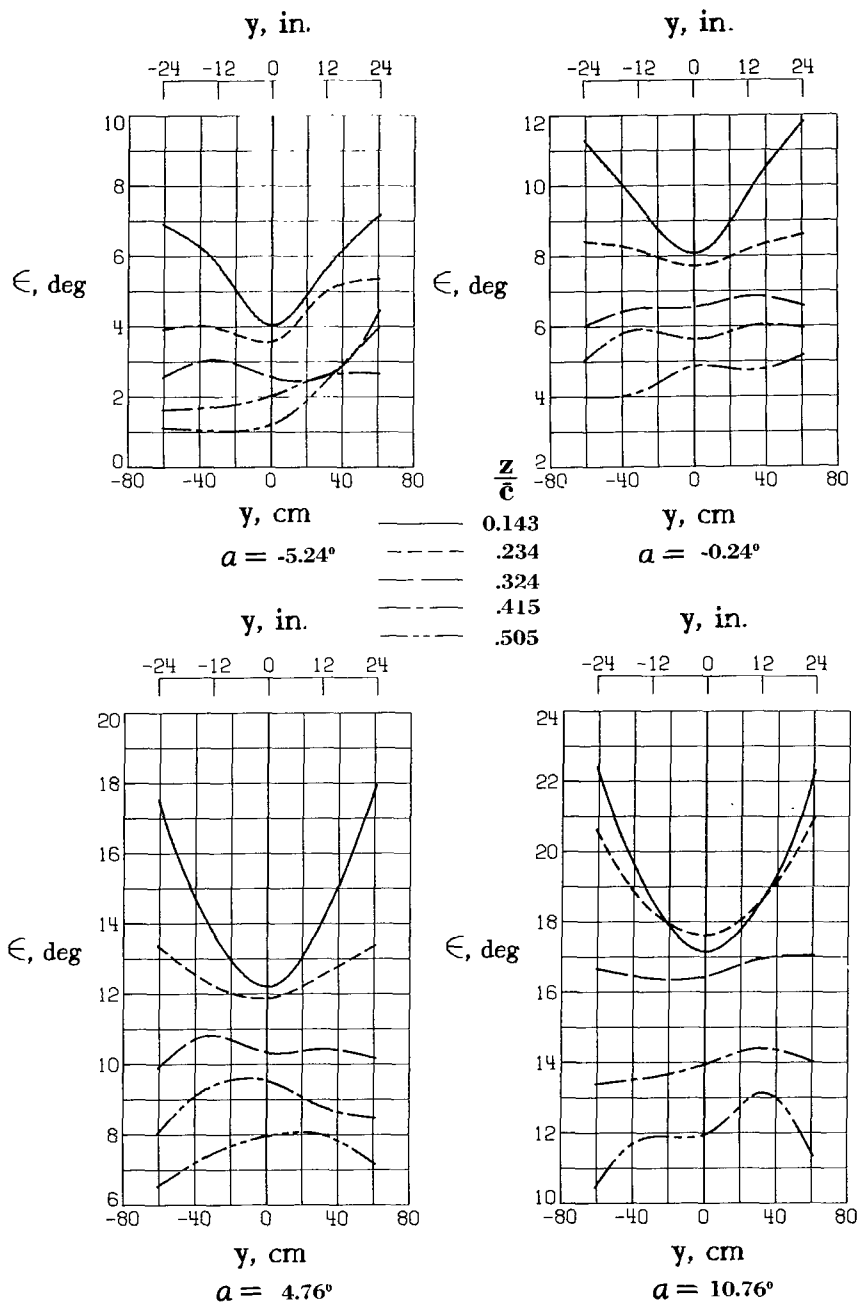
(a) $T_c' = 0.2$; $l/\bar{c} = 0.982$.

Figure 14.- Variation of downwash angle with spanwise station.
$\delta_f = 20°$. Deflectors on.

38

y, in.

y, in.

$\in$, deg

$\in$, deg

$a = -5.24°$

$a = -0.24°$

$\frac{z}{\bar{c}}$

——— 0.143
----- .234
—— .324
—·—· .415
—··—·· .505

y, cm

y, cm

y, in.

y, in.

$\in$, deg

$\in$, deg

y, cm

y, cm

$a = 4.76°$

$a = 10.76°$
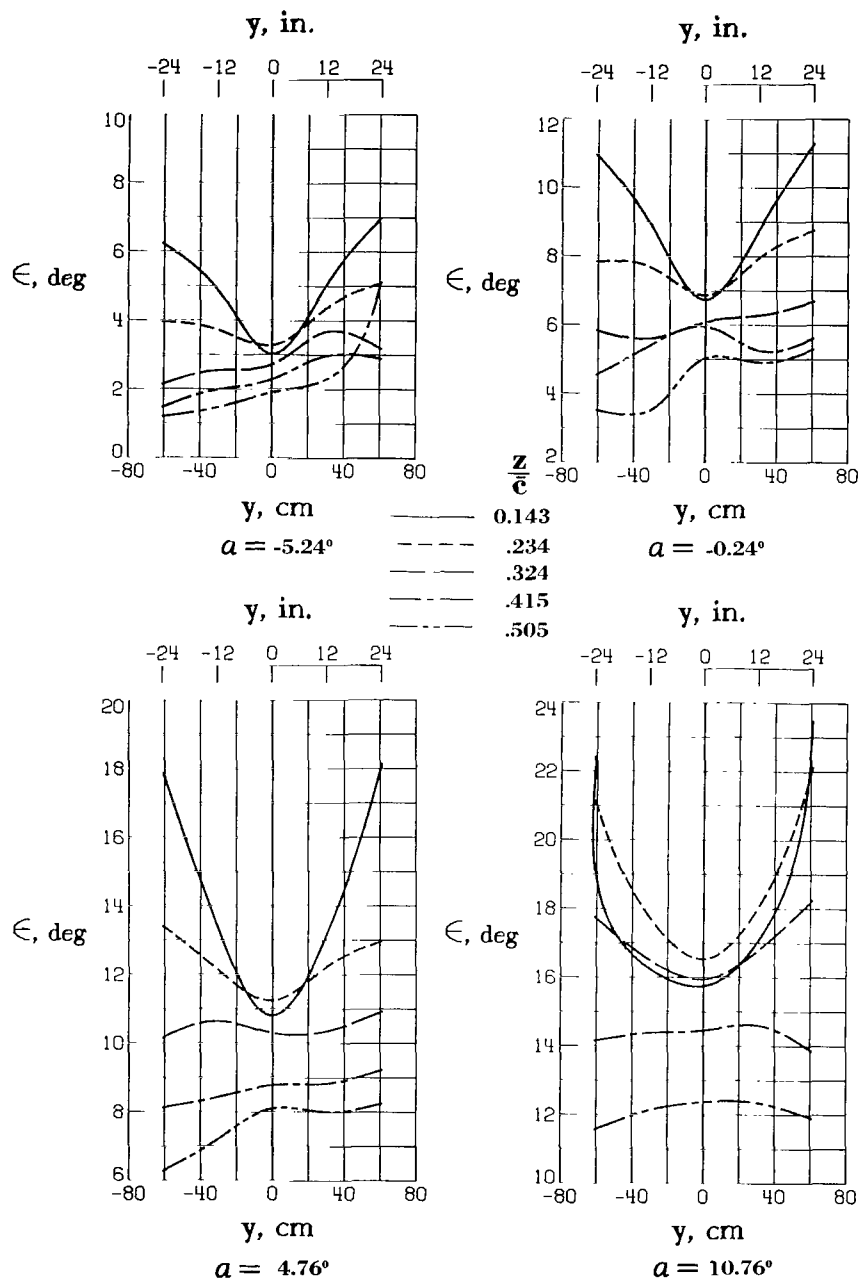
(b) $T_c' = 0.20$; $l/\bar{c} = 1.254$.

Figure 14.- Concluded.

$1 - \dfrac{d\epsilon}{d\alpha}$

$\dfrac{Z}{\bar{c}}$

T_c^1	Deflector
0	Off
.2	Off
.2	On

(a) $l/\bar{c}$ = 0.982.

$1 - \dfrac{d\epsilon}{d\alpha}$

$\dfrac{Z}{\bar{c}}$
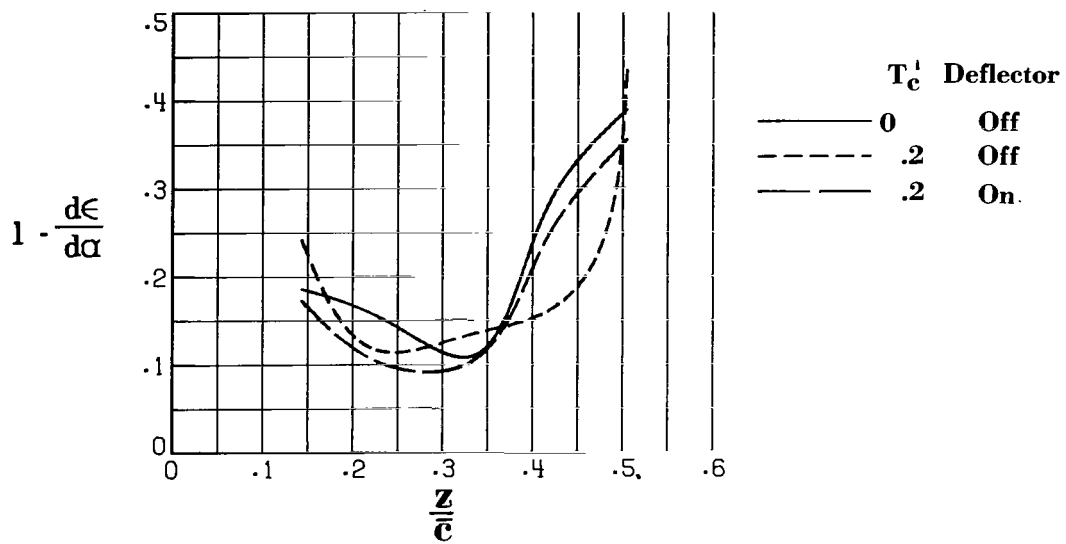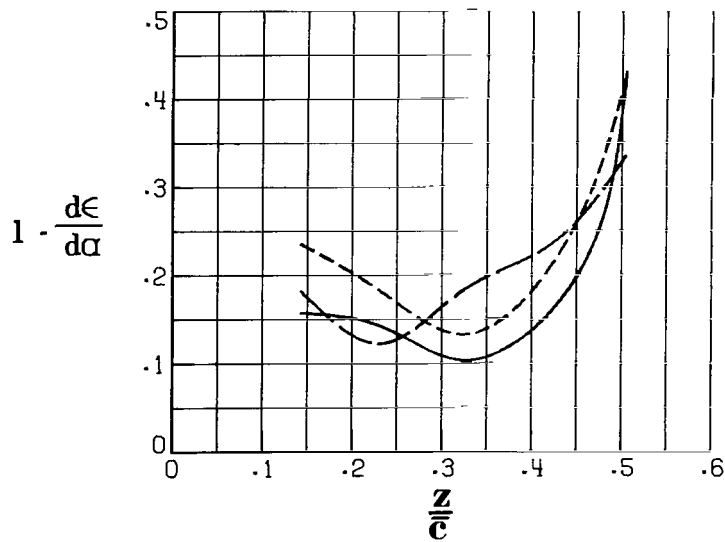
(b) $l/\bar{c}$ = 1.254.

Figure 15.- Variation of downwash factor for various tail positions, tail heights, and thrust coefficients. $\delta_f = 20^{\circ}$.

(a) $T_c' = 0^o$.
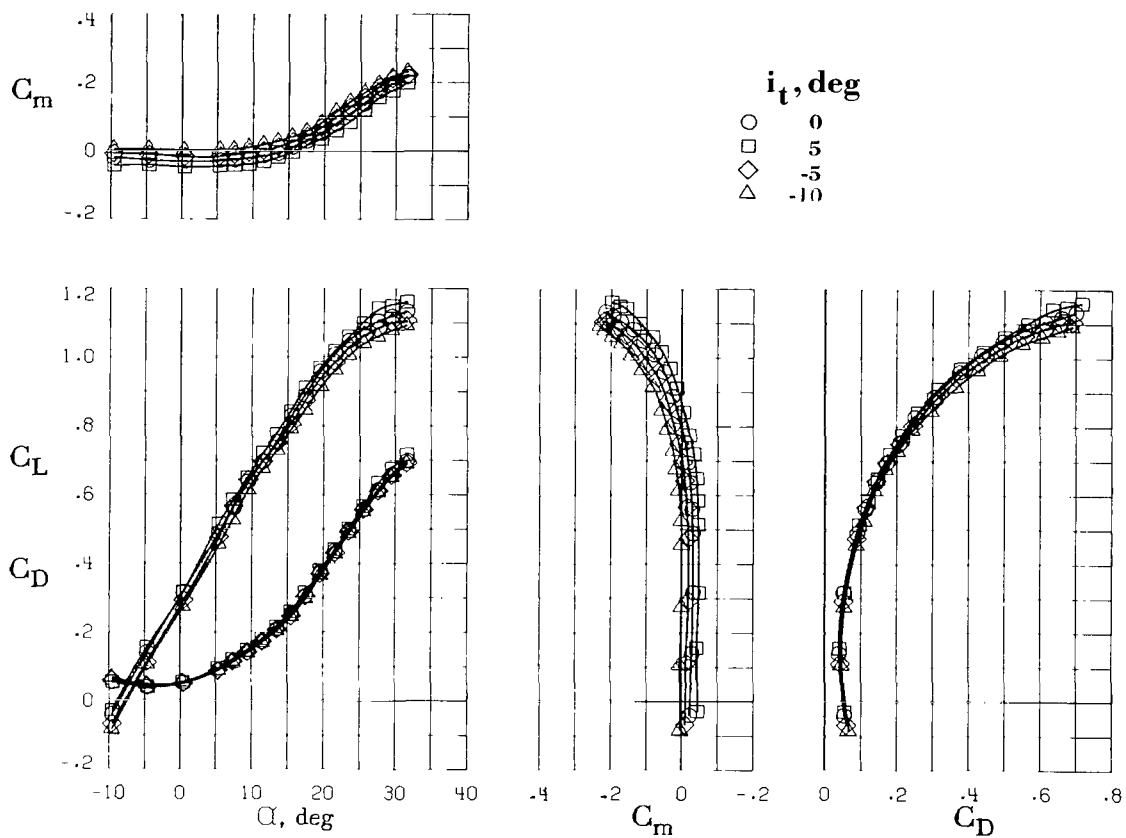
Figure 16.- Effect of tail incidence on the longitudinal aerodynamic characteristics for various thrust conditions. $\delta_f = 30^o$; 20° exhaust deflectors installed; T-tail installed.
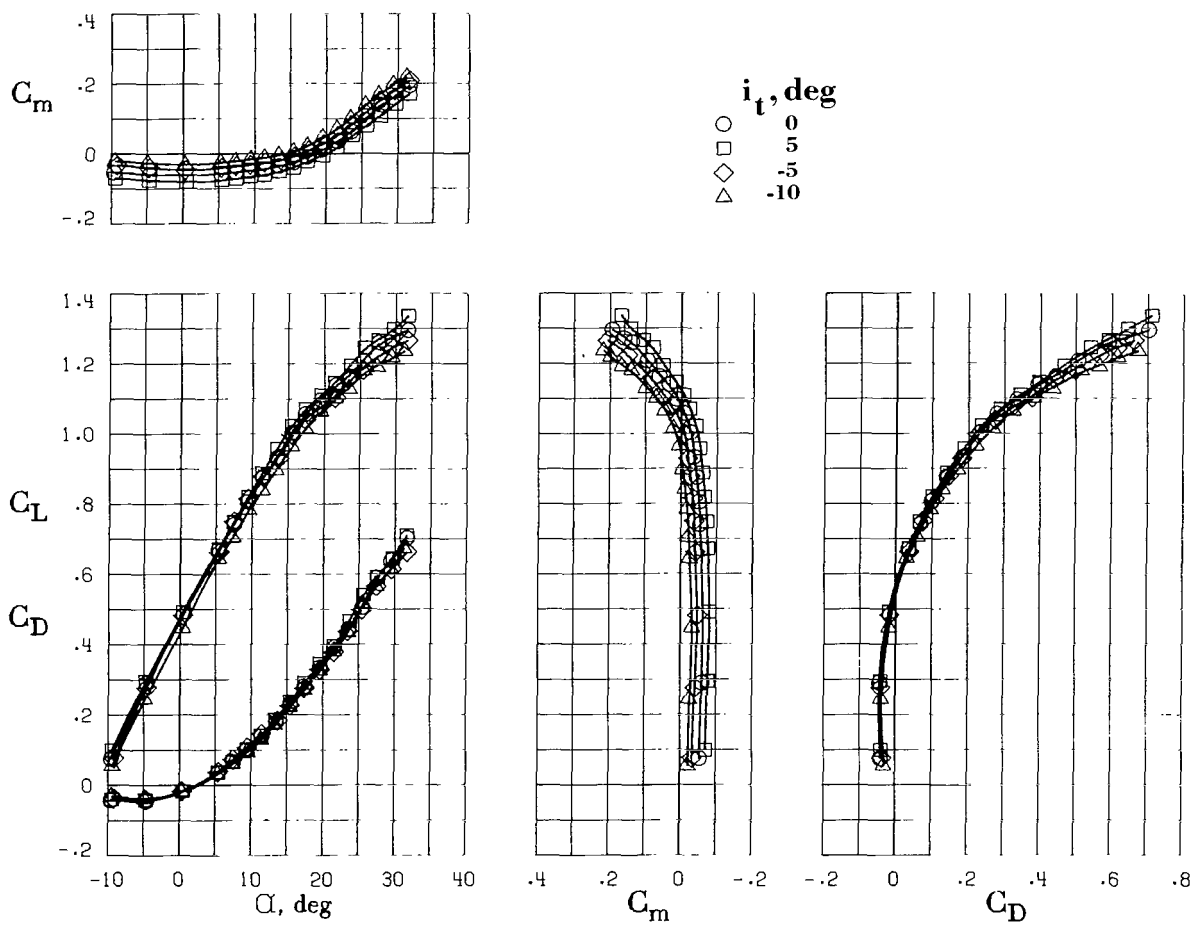
(b) $T_c' = 0.1$.

Figure 16.- Continued.
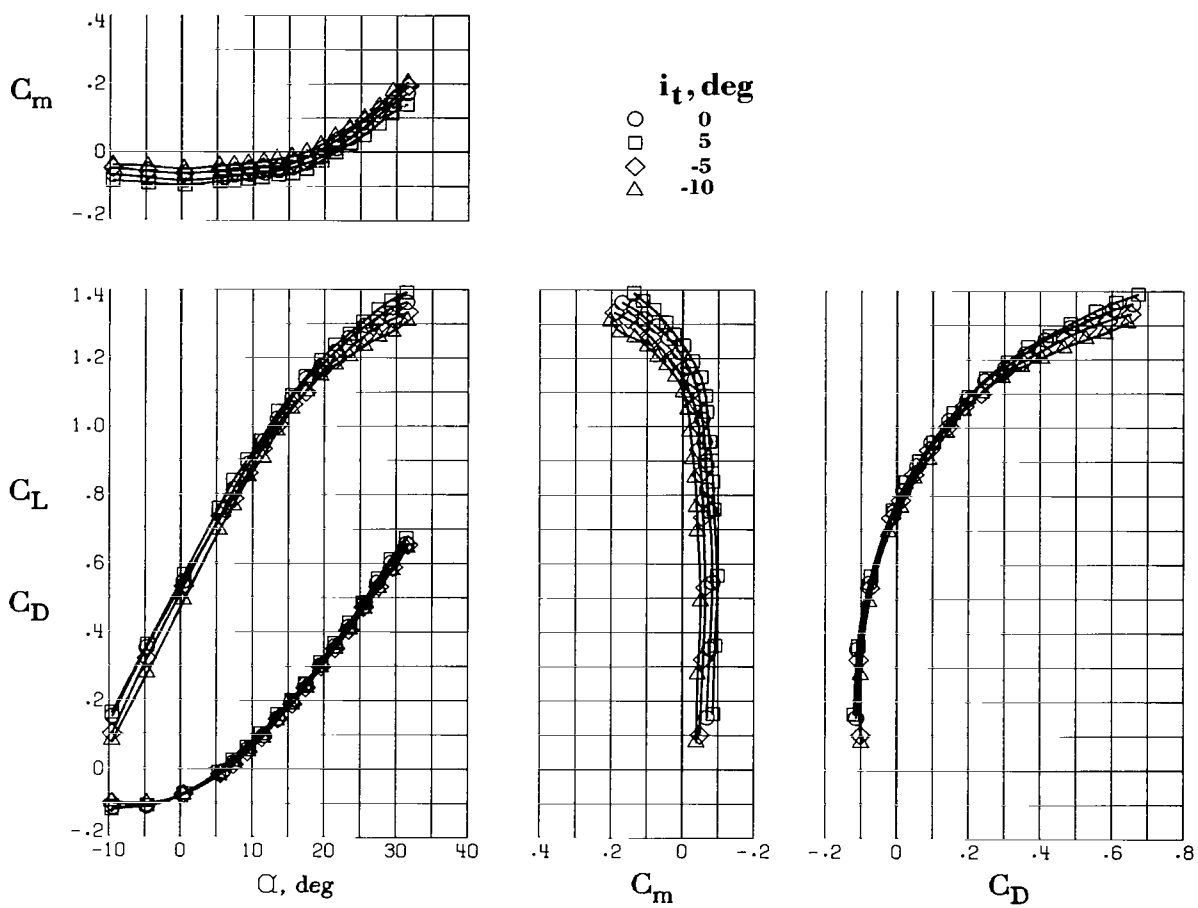
(c) $T_c' = 0.2$.

Figure 16.- Concluded.
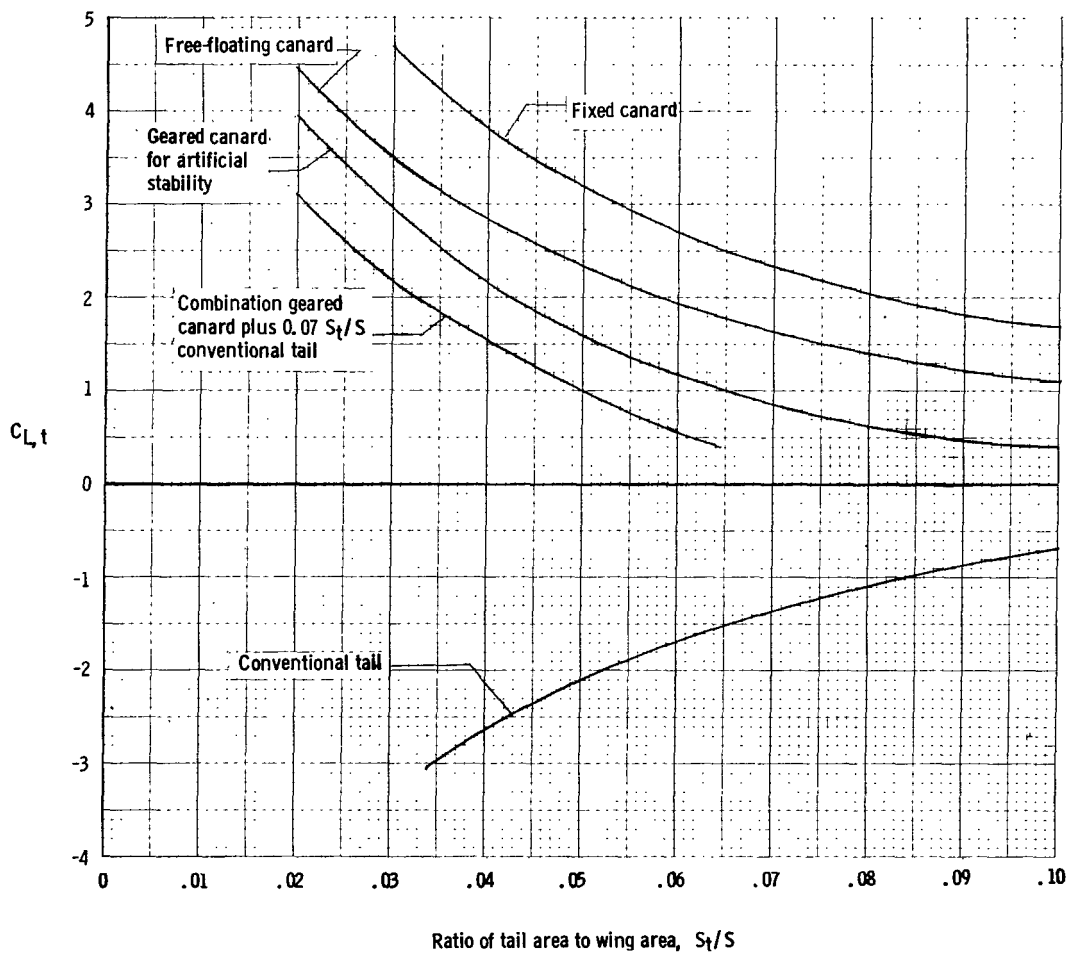
(a) Variation of trim lift coefficient with S_t/S.

Figure 17.- Comparison of several methods of achieving pitch trim and longitudinal stability. $\delta_f = 30^{\circ}$.
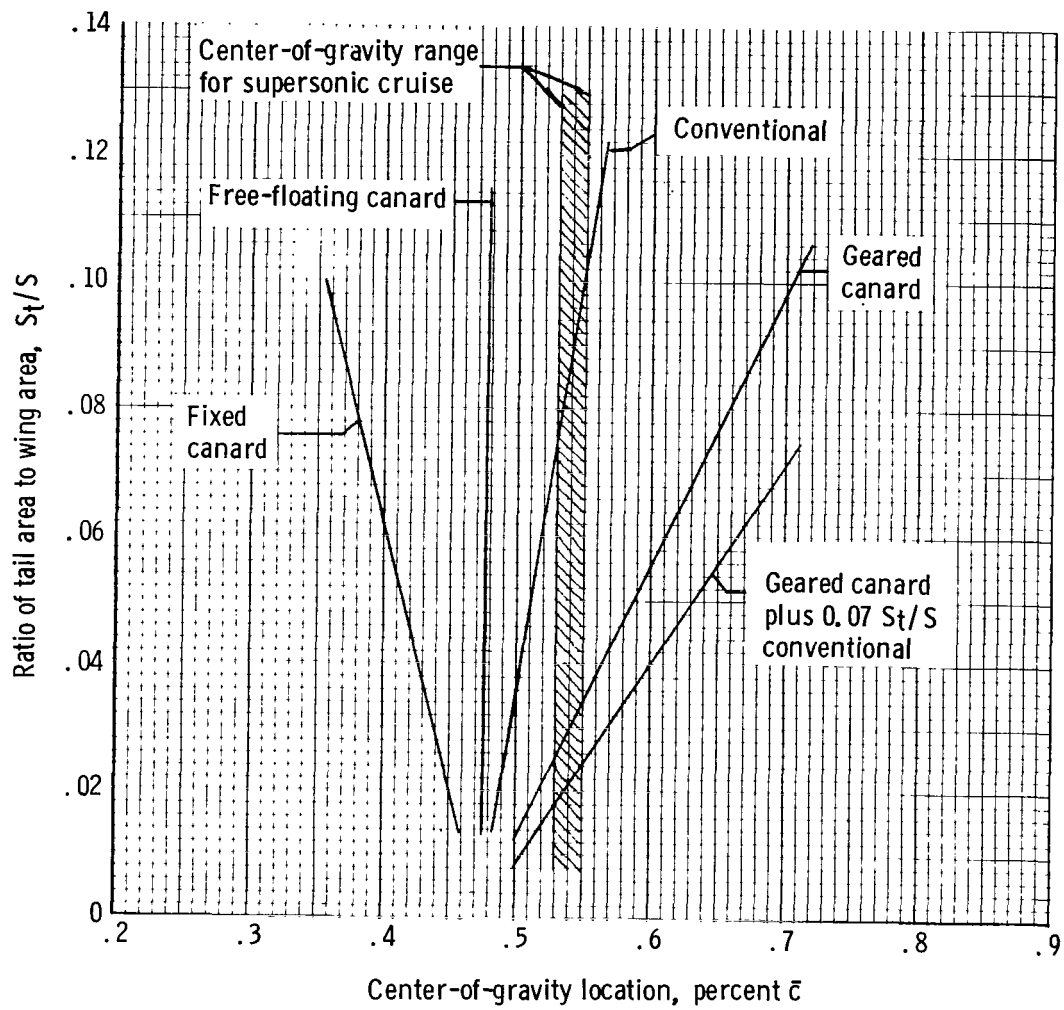
(b) Variation of center-of-gravity location with S_t/S.

Figure 17.- Concluded.
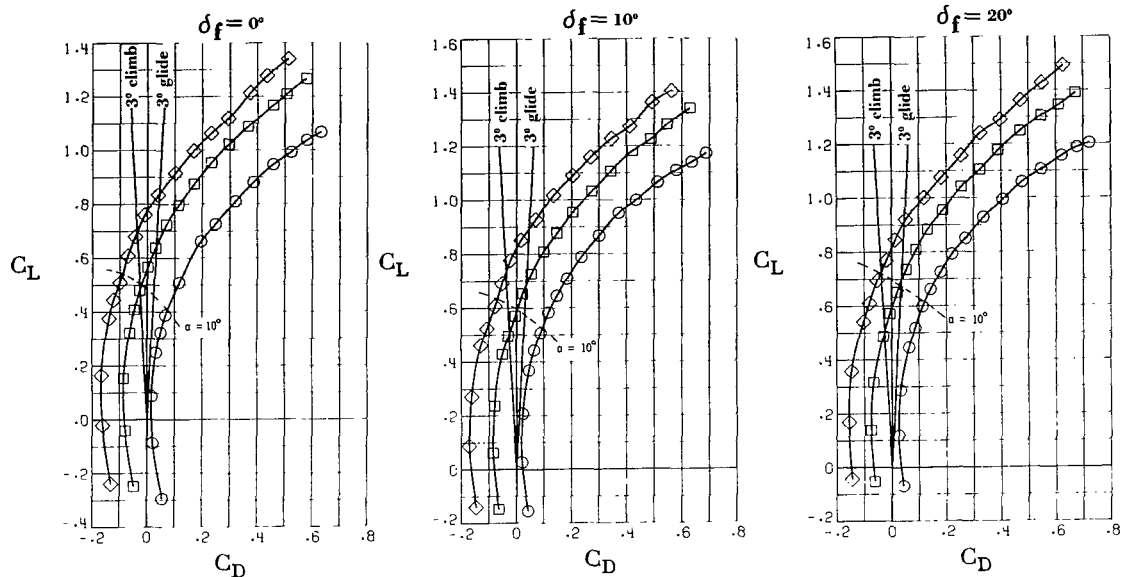
(a) No exhaust deflector installed.
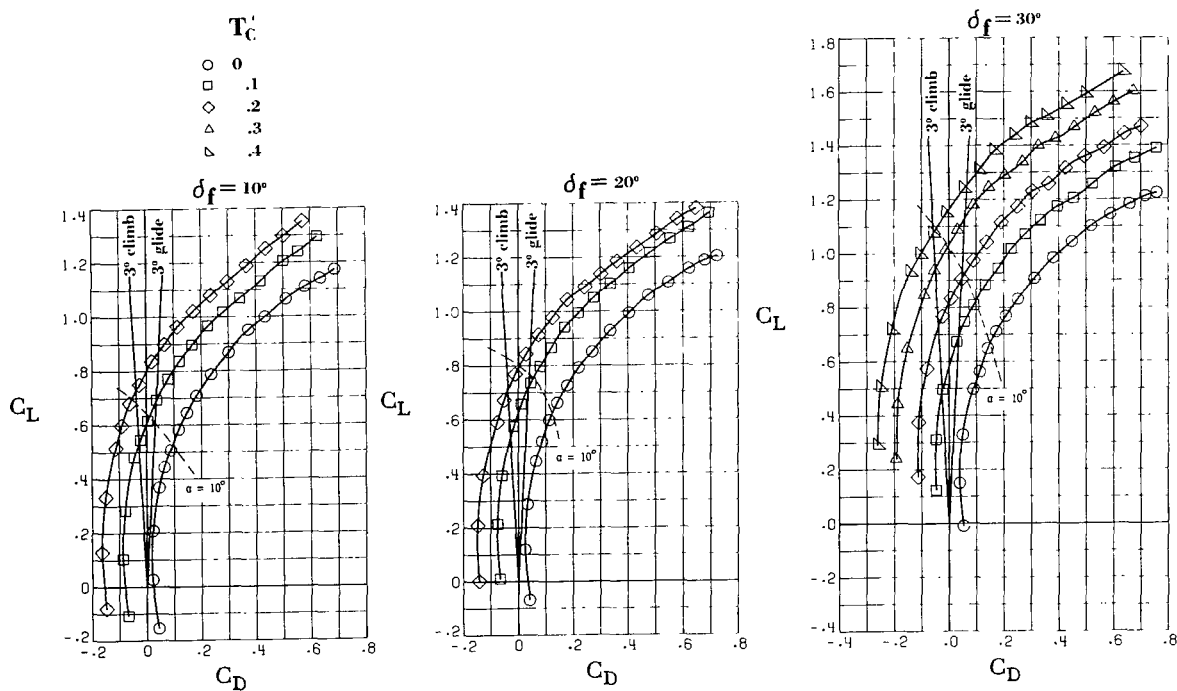
(b) 20° exhaust deflectors installed.

Figure 18.- Effect of exhaust deflectors on the lift-drag polars for various flap settings.

(a) No exhaust deflector installed.　　　(b) 20° exhaust deflectors installed.

Figure 19.- Effect of exhaust deflectors on T/W against C_L for various flap deflections.
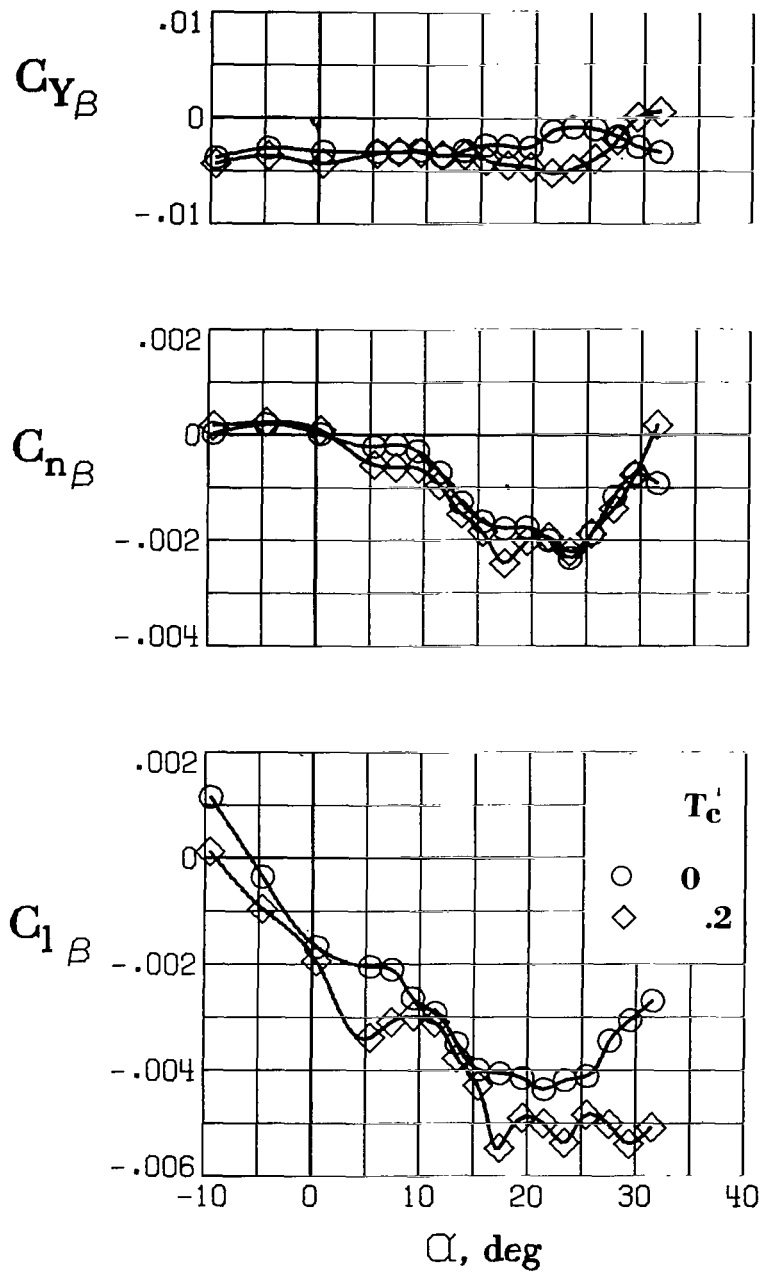
(a) Tail off.

Figure 20.- Effect of thrust coefficient on the static lateral-directional stability derivatives. 20° exhaust deflectors installed; $\delta_f = 30^{\circ}$.
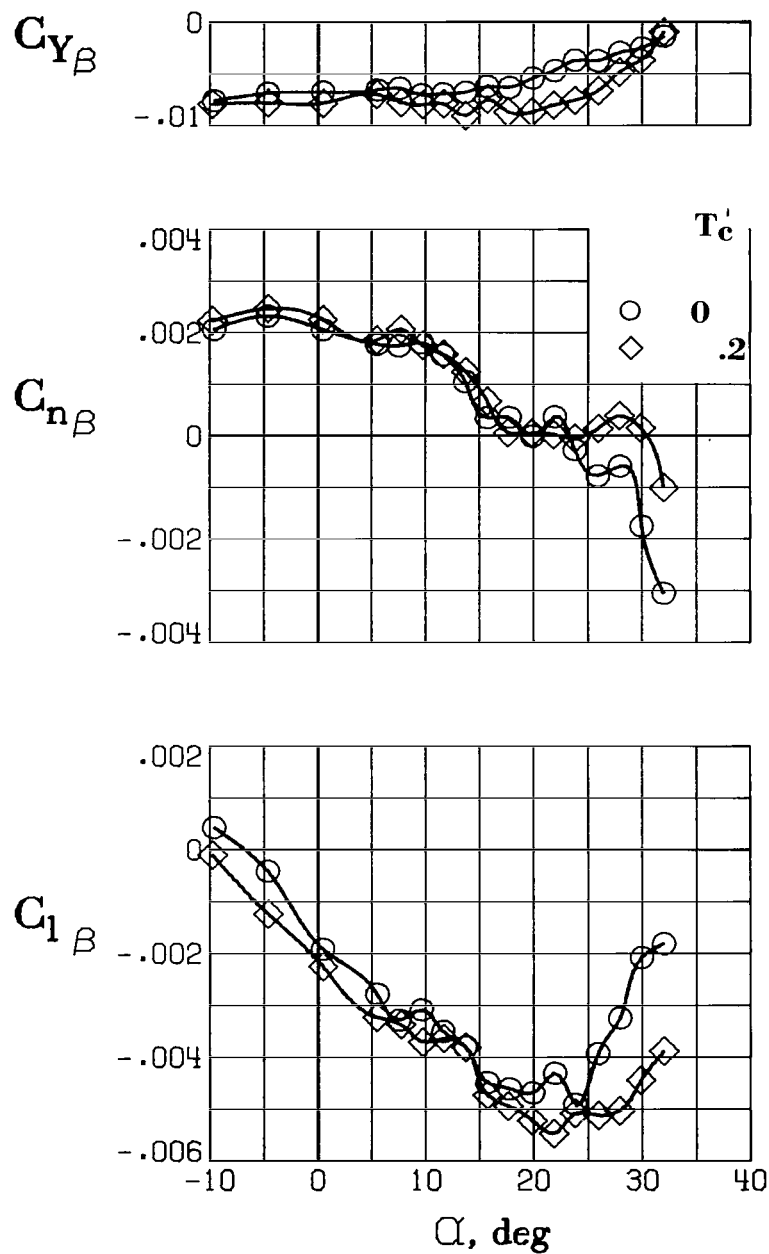
(b) Tail on.

Figure 20.- Concluded.
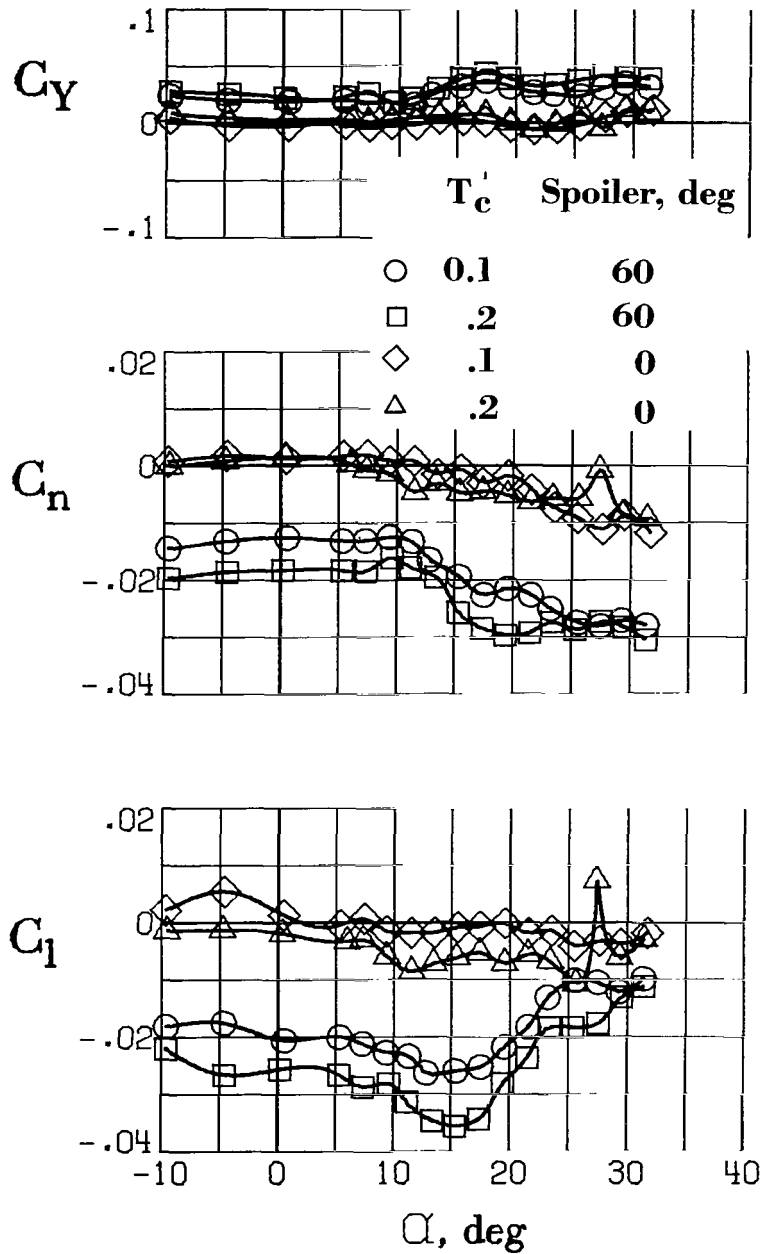
(a) Lateral-directional characteristics.

Figure 21.- Effect of spoilers on the static lateral and longitudinal aerodynamic characteristics for various thrust coefficients. 20° exhaust deflectors installed. $\delta_f = 30^O$. T-tail on.
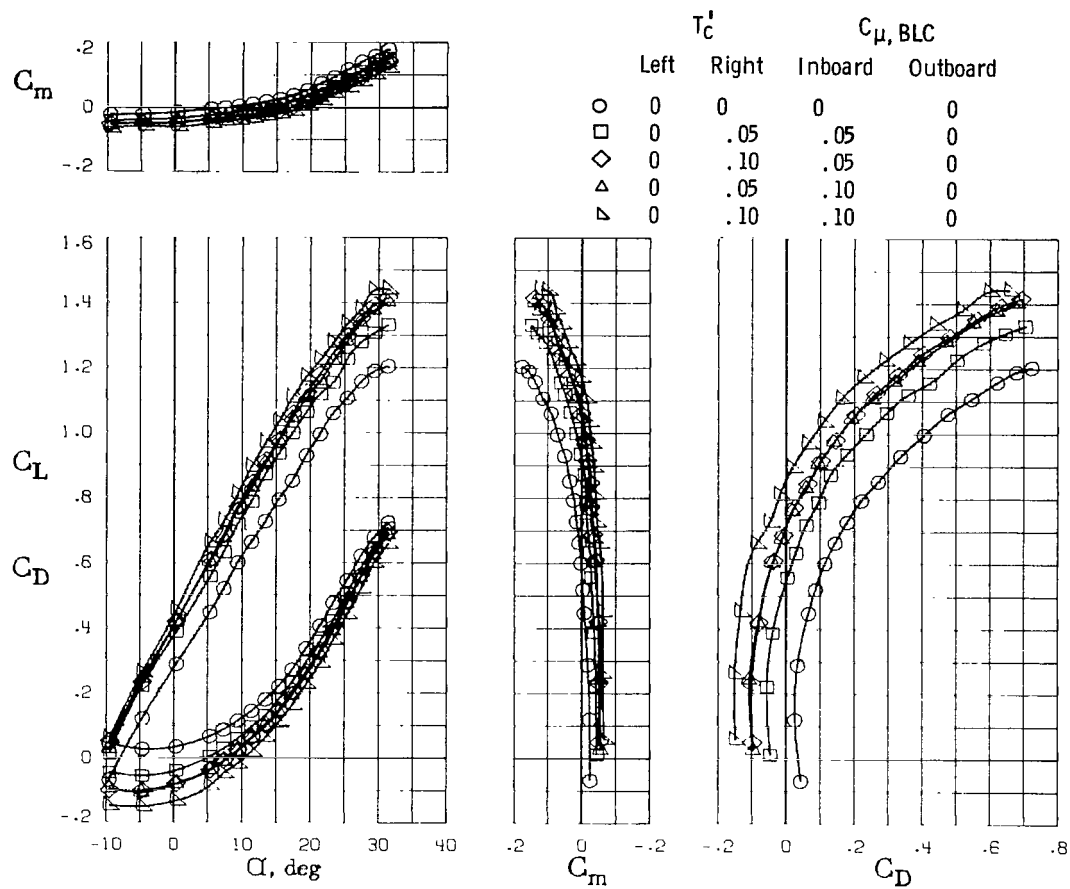
	T_c'	Spoiler, deg
○	0.1	60
□	.2	60
◇	.1	0
△	.2	0
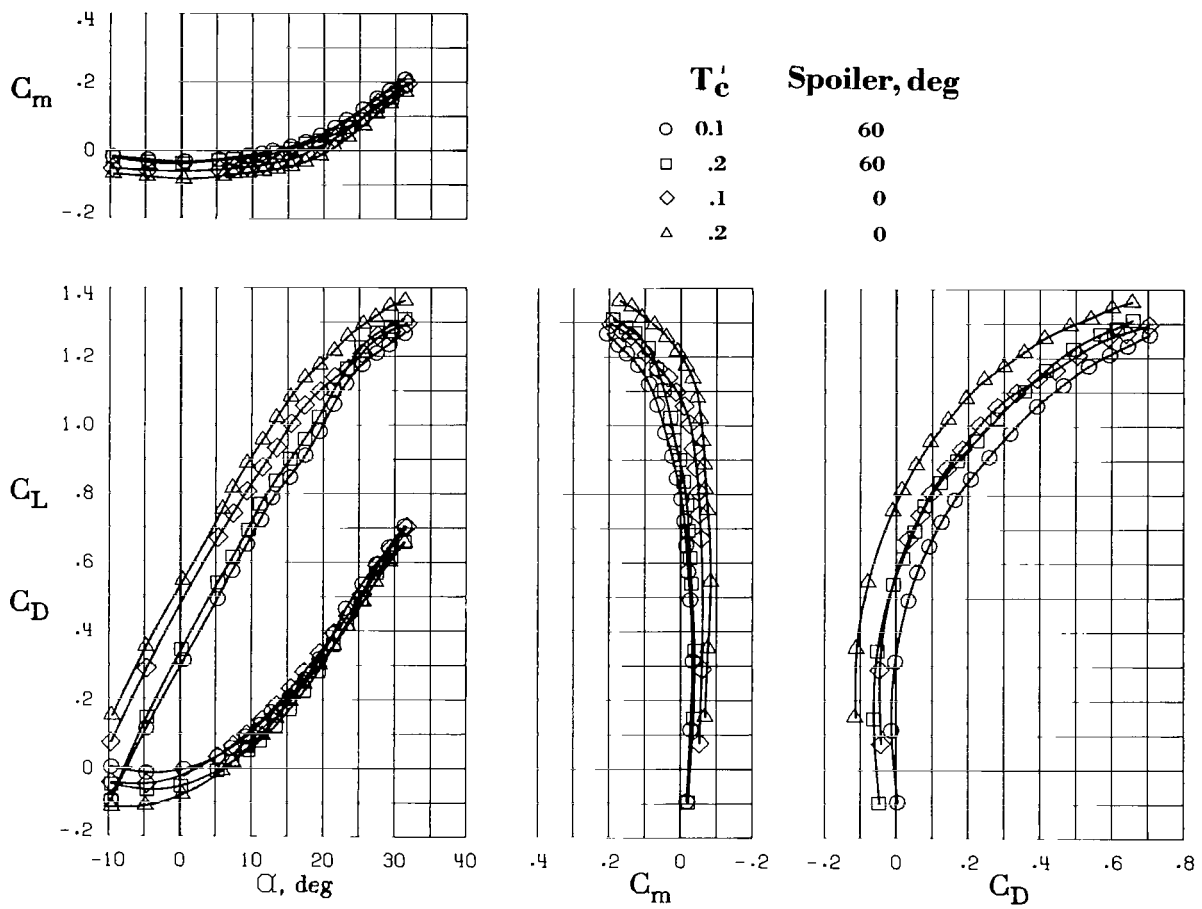
(b) Longitudinal characteristics.

Figure 21.- Concluded.
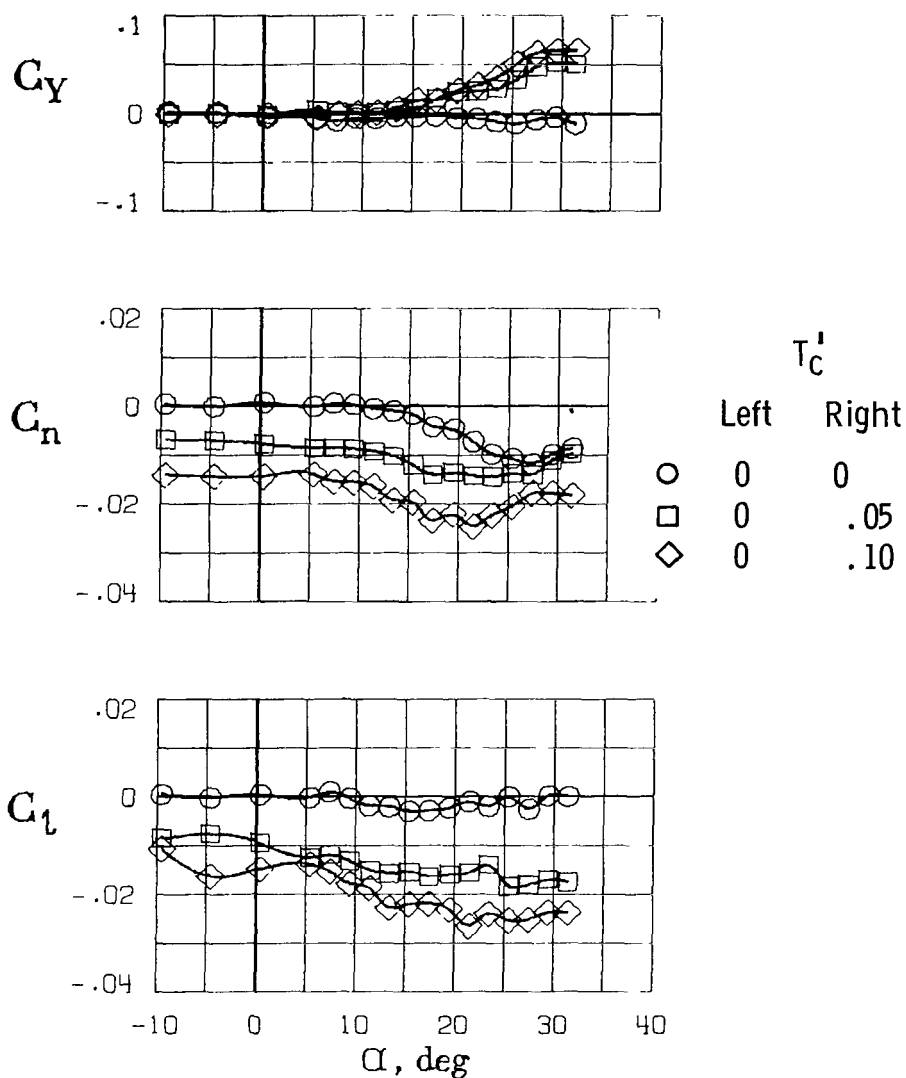
(a) Lateral-directional characteristics.

Figure 22.- Effect of one engine inoperative on the static lateral and longitudinal aerodynamic characteristics for various thrust coefficients. 20° exhaust deflectors installed; $\delta_f = 20^{\circ}$.
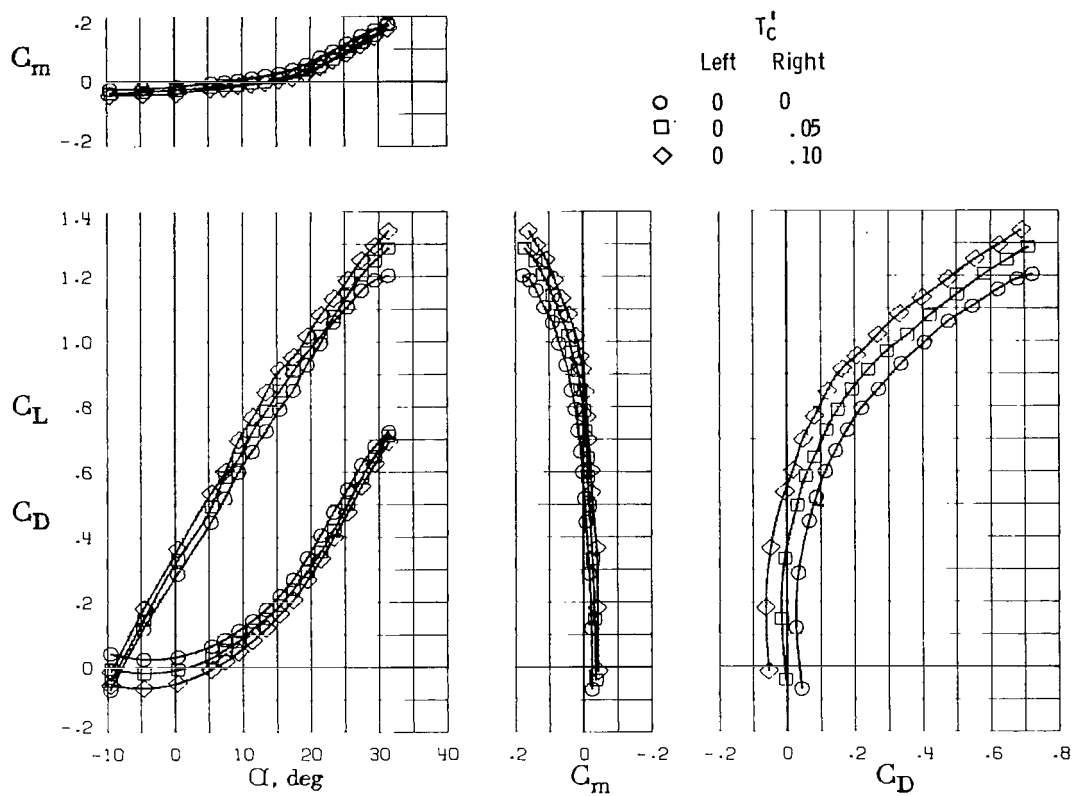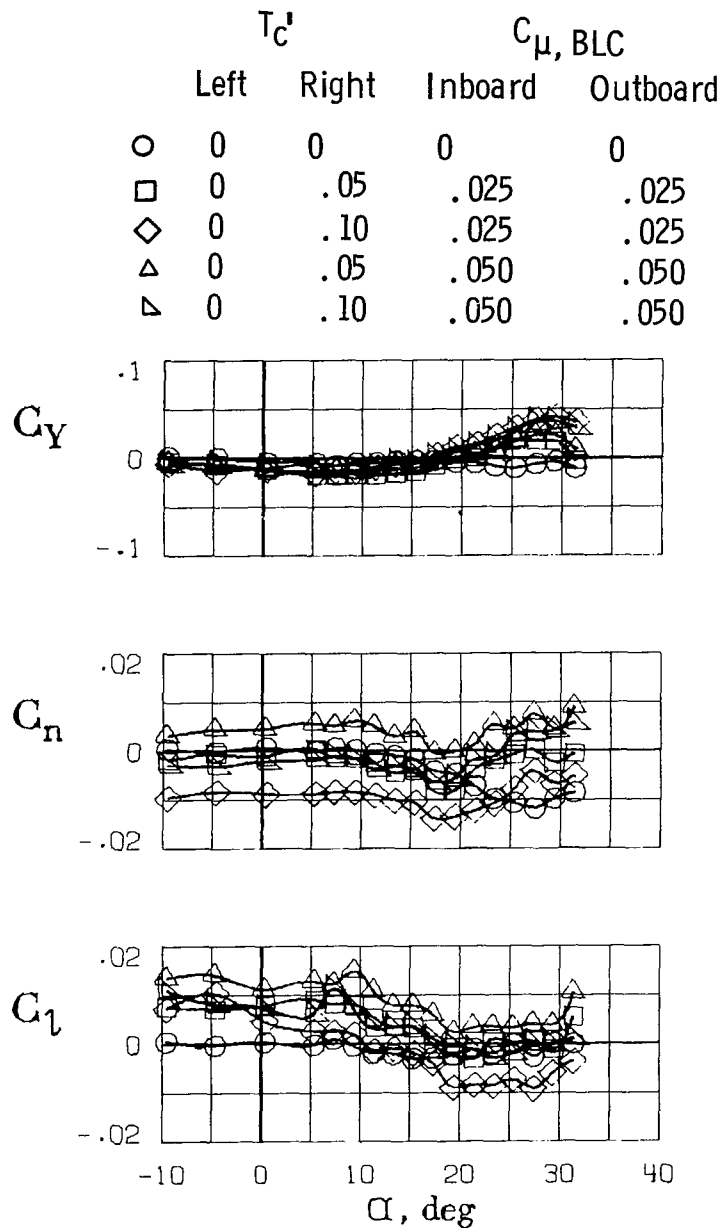
(b) Longitudinal characteristics.

Figure 22.- Concluded.
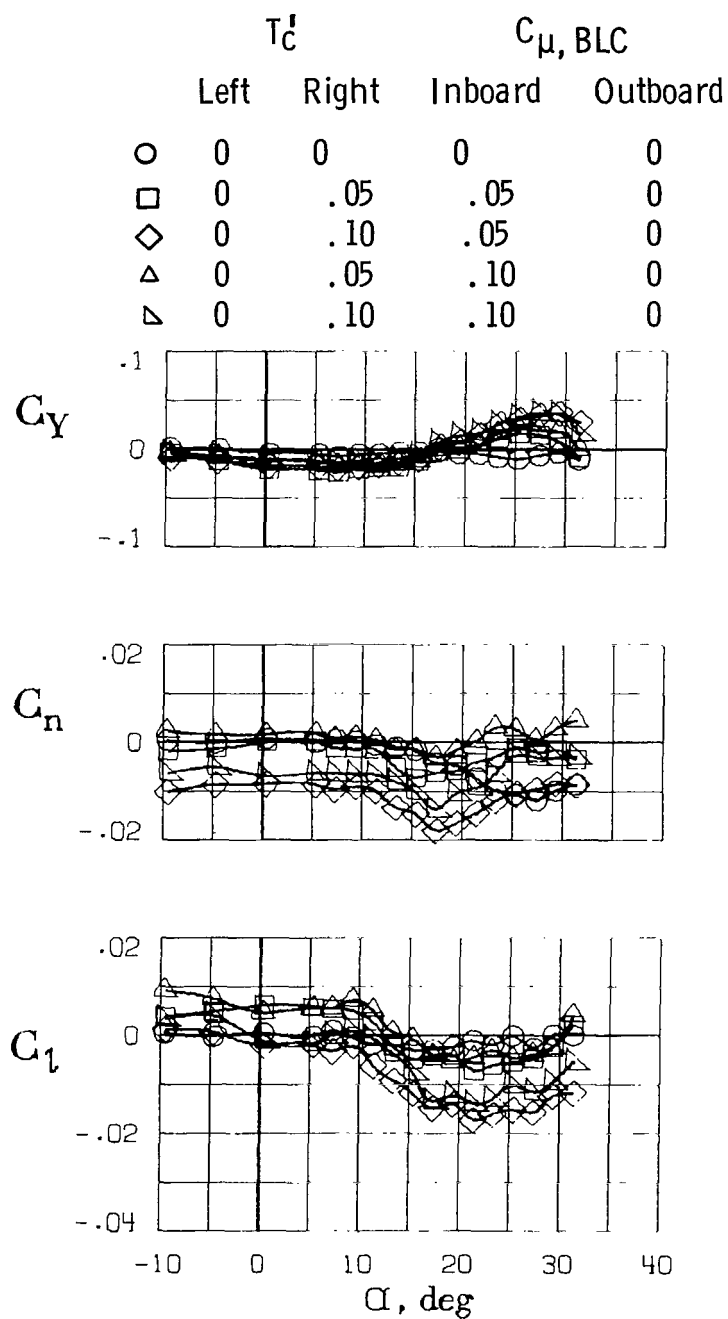
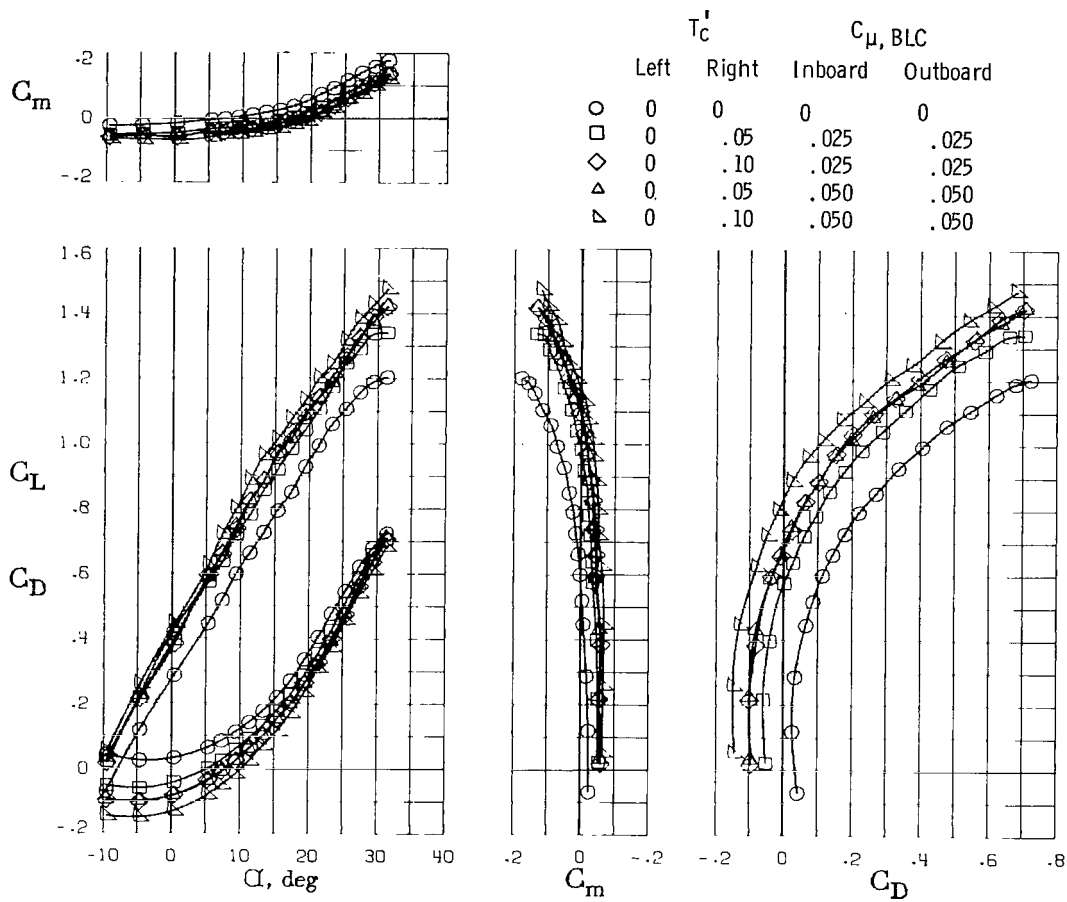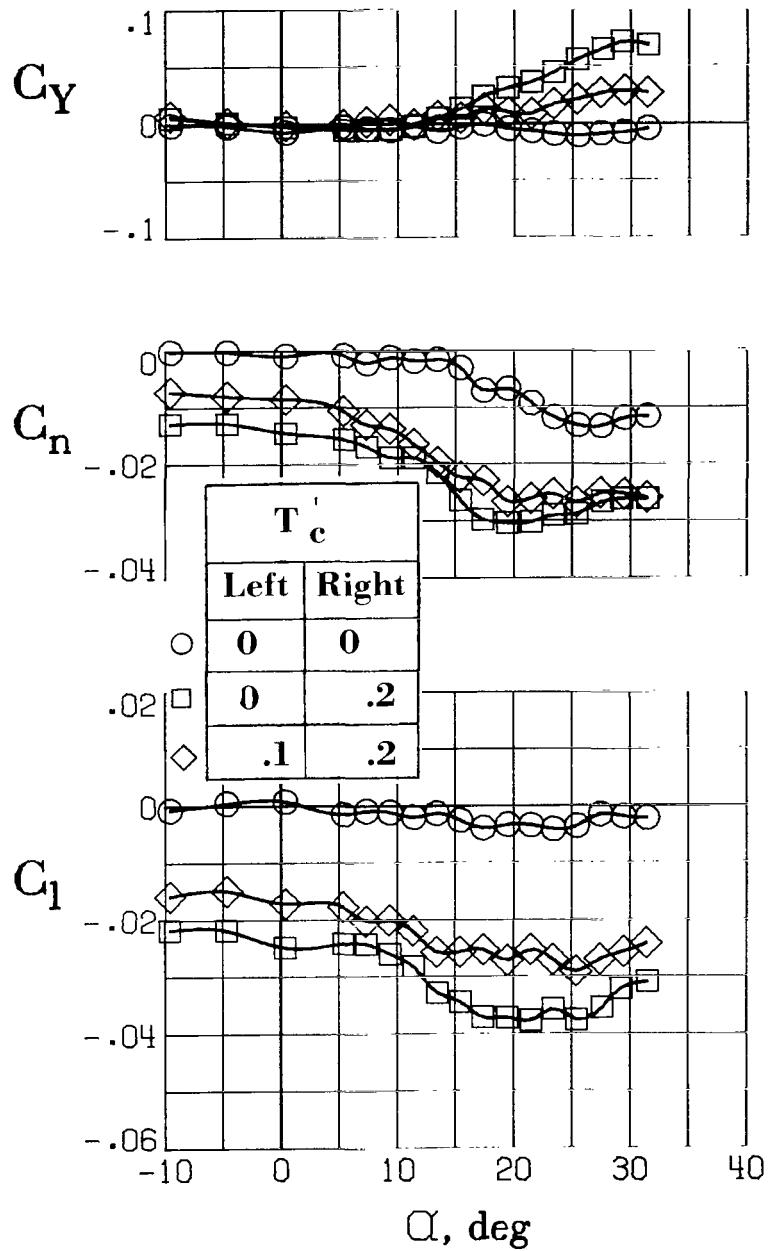(a) Lateral-directional characteristics.

Figure 23.- Effect of asymmetric boundary-layer control on the static lateral and longitudinal aerodynamic characteristics for various thrust and blowing coefficients. $20°$ exhaust deflectors installed; $\delta_f = 20°$.

(b) Longitudinal characteristics.

Figure 23.- Concluded.

	T_c'		$C_{\mu, BLC}$	
	Left	Right	Inboard	Outboard
○	0	0	0	0
□	0	.05	.025	.025
◇	0	.10	.025	.025
△	0	.05	.050	.050
◿	0	.10	.050	.050

(a) Lateral-directional characteristics.

Figure 24.- Effect of asymmetric boundary-layer control on the static lateral and longitudinal aerodynamic characteristics for various thrust and blowing coefficients. 20° exhaust deflectors installed; $\delta_f = 20^{\circ}$.

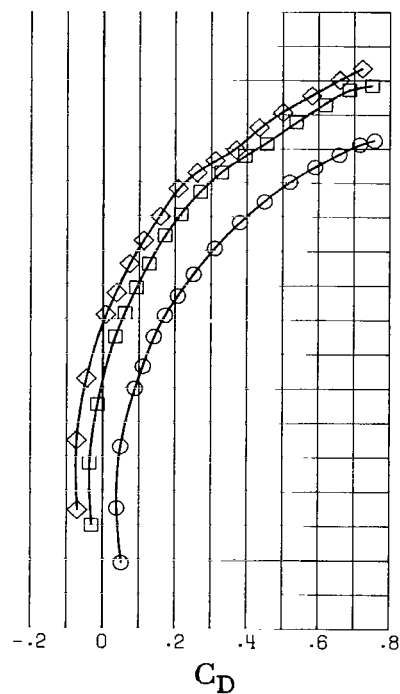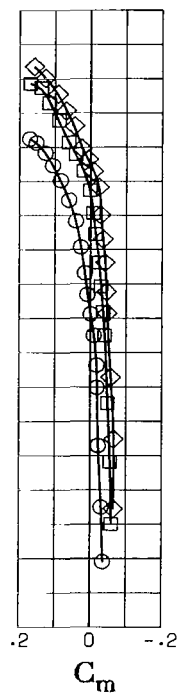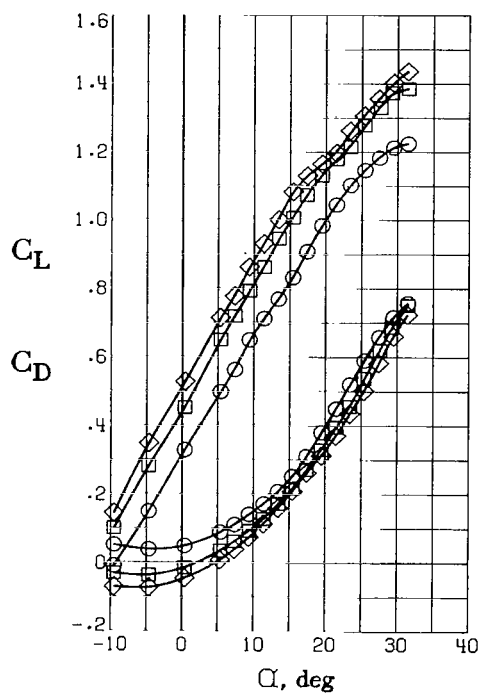(b) Longitudinal characteristics.

Figure 24.- Concluded.

(a) Lateral-directional characteristics.

Figure 25.- Effect of asymmetric engine thrust coefficients on the static lateral and longitudinal aerodynamic characteristics. 20° exhaust deflectors installed; $\delta_f = 30^{\circ}$.
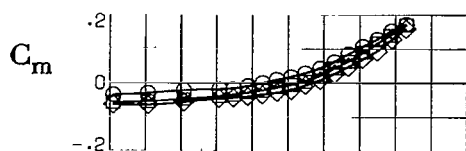
(b) Longitudinal characteristics.

Figure 25.- Concluded.

"The aeronautical and space activities of the United States shall be conducted so as to contribute . . . to the expansion of human knowledge of phenomena in the atmosphere and space. The Administration shall provide for the widest practicable and appropriate dissemination of information concerning its activities and the results thereof."
—NATIONAL AERONAUTICS AND SPACE ACT OF 1958

NASA SCIENTIFIC AND TECHNICAL PUBLICATIONS

TECHNICAL REPORTS: Scientific and technical information considered important, complete, and a lasting contribution to existing knowledge.

TECHNICAL NOTES: Information less broad in scope but nevertheless of importance as a contribution to existing knowledge.

TECHNICAL MEMORANDUMS: Information receiving limited distribution because of preliminary data, security classification, or other reasons. Also includes conference proceedings with either limited or unlimited distribution.

CONTRACTOR REPORTS: Scientific and technical information generated under a NASA contract or grant and considered an important contribution to existing knowledge.

TECHNICAL TRANSLATIONS: Information published in a foreign language considered to merit NASA distribution in English.

SPECIAL PUBLICATIONS: Information derived from or of value to NASA activities. Publications include final reports of major projects, monographs, data compilations, handbooks, sourcebooks, and special bibliographies.

TECHNOLOGY UTILIZATION PUBLICATIONS: Information on technology used by NASA that may be of particular interest in commercial and other non-aerospace applications. Publications include Tech Briefs, Technology Utilization Reports and Technology Surveys.

Details on the availability of these publications may be obtained from:

SCIENTIFIC AND TECHNICAL INFORMATION OFFICE

NATIONAL AERONAUTICS AND SPACE ADMINISTRATION
Washington, D.C. 20546